NASA/CR—2003-212320

Enhanced Mixing in a Rectangular Duct

D.S. Liscinsky and B. True
Pratt & Whitney, East Hartford, Connecticut

June 2003

The NASA STI Program Office . . . in Profile

Since its founding, NASA has been dedicated to the advancement of aeronautics and space science. The NASA Scientific and Technical Information (STI) Program Office plays a key part in helping NASA maintain this important role.

The NASA STI Program Office is operated by Langley Research Center, the Lead Center for NASA's scientific and technical information. The NASA STI Program Office provides access to the NASA STI Database, the largest collection of aeronautical and space science STI in the world. The Program Office is also NASA's institutional mechanism for disseminating the results of its research and development activities. These results are published by NASA in the NASA STI Report Series, which includes the following report types:

- TECHNICAL PUBLICATION. Reports of completed research or a major significant phase of research that present the results of NASA programs and include extensive data or theoretical analysis. Includes compilations of significant scientific and technical data and information deemed to be of continuing reference value. NASA's counterpart of peer-reviewed formal professional papers but has less stringent limitations on manuscript length and extent of graphic presentations.

- TECHNICAL MEMORANDUM. Scientific and technical findings that are preliminary or of specialized interest, e.g., quick release reports, working papers, and bibliographies that contain minimal annotation. Does not contain extensive analysis.

- CONTRACTOR REPORT. Scientific and technical findings by NASA-sponsored contractors and grantees.

- CONFERENCE PUBLICATION. Collected papers from scientific and technical conferences, symposia, seminars, or other meetings sponsored or cosponsored by NASA.

- SPECIAL PUBLICATION. Scientific, technical, or historical information from NASA programs, projects, and missions, often concerned with subjects having substantial public interest.

- TECHNICAL TRANSLATION. English-language translations of foreign scientific and technical material pertinent to NASA's mission.

Specialized services that complement the STI Program Office's diverse offerings include creating custom thesauri, building customized databases, organizing and publishing research results . . . even providing videos.

For more information about the NASA STI Program Office, see the following:

- Access the NASA STI Program Home Page at ***http://www.sti.nasa.gov***

- E-mail your question via the Internet to help@sti.nasa.gov

- Fax your question to the NASA Access Help Desk at 301–621–0134

- Telephone the NASA Access Help Desk at 301–621–0390

- Write to:
  NASA Access Help Desk
  NASA Center for AeroSpace Information
  7121 Standard Drive
  Hanover, MD 21076

NASA/CR—2003-212320

Enhanced Mixing in a Rectangular Duct

D.S. Liscinsky and B. True
Pratt & Whitney, East Hartford, Connecticut

Prepared under Contract NAS3–25954, Task Order 12

National Aeronautics and
Space Administration

Glenn Research Center

June 2003

Document Notice

This reseach was originally published internally as HSR047 in March 1997.

Trade names or manufacturers' names are used in this report for identification only. This usage does not constitute an official endorsement, either expressed or implied, by the National Aeronautics and Space Administration.

Available from

NASA Center for Aerospace Information
7121 Standard Drive
Hanover, MD 21076

National Technical Information Service
5285 Port Royal Road
Springfield, VA 22100

Available electronically at http://gltrs.grc.nasa.gov

Contents

ENHANCED MIXING IN A RECTANGULAR DUCT
Contents iii

List of Symbols v

1. Introduction 1

2. Approach 2

3. Experimental 4
3.1 Apparatus 4

3.2 Data Acquisition 4

4. Results and Discussion 6
4.1 Review of Previous Work (Concept 1 Configurations) 6

4.2 Concept 2 Configurations 7
4.2.1 Orifice Spacing 8
4.2.2 Orifice Diameter and Blockage 10
4.2.3 Inline vs. Staggered 12

4.3 Concept 3 Configurations 14

4.4 Effects of Initial Conditions 16
4.4.1 Approach Profile 16
4.4.2 Contraction of the Mainstream 17
4.4.3 Jet Delivery System 19
4.4.4 Upstream Swirl 21

4.5 Blockage Revisited 22

4.6 NO_x Inference Data Sets 26

4.7 Non-Circular Single Jets 29

4. Conclusions 39

5. References 40

List of Symbols

A_j/A_m	jet-to-mainstream area ratio = $(\pi/2)\ (S/H)\ /\ (S/d)^2$
B	blockage = y projection / S
C	$(S/H) * \sqrt{J}$ (see Eq. 3)
$\bar{c}$	fully mixed mass fraction = MR /(1 + MR) = θ_{EB}, Ref.8)
C_d	orifice discharge coefficient
d	orifice diameter
H	duct height at injection plane
J	jet-to-mainstream momentum-flux ratio = $(\rho_j\ V_j^2)\ /\ (\rho_m\ V_m^2)$
ρ	density
S	spacing between adjacent orifice mid-points
U_s	spatial unmixedness parameter (Eq. 2)
V_m	mainstream velocity
V_j	jet velocity $= w_j\ /\ \rho_j\ A_j C_d$
MR	jet-to-mainstream mass flow ratio
x	downstream coordinate, x = 0 at the upstream edge of the orifice
y	cross-stream coordinate

1. Introduction

This study began in 1990 as part of NASA's High Speed Research Program aimed at determining the feasibility of a High Speed Civil Transport (HSCT). The environmental acceptability of this type of airplane is a key issue and the technology reported herein addresses the reduction of NO_x emissions from a candidate propulsion system. Comprehensive review of the background of the HSCT initiative, NO_x chemistry, and low NO_x combustor concepts can be found in Shaw[1] and Jones[2] among others and therefore is not repeated here.

An advanced low NO_x engine based on a Rich-burn/Quick-mix/Lean-burn(RQL) combustor is one of the concepts that has been proposed to power the HSCT. An advantage of the RQL combustor is excellent stability due to its rich primary zone, however low emissions depend on an efficient quick mix section that rapidly and uniformly dilutes the rich zone products to minimize NO_x in the exhaust. The injection of jets normal to the main flow of the combustor is under evaluation as a key technology for the development of the RQL engine concept. This commonly employed mixing technique is found in the dilution zone of conventional gas turbine combustors, which typically use rows of relatively cool air jets to lower the exit temperature of the combustor. Extensive cross flow mixing investigations reported by Holdeman[3] have focussed on conventional gas turbine dilution zones where up to 30% of the total flow was introduced with the dilution jets. Recently other studies of jets in a rectangular cross flow have been reported[4-33]. These studies all conclude that the rate of mixing by a row of jets in cross flow is primarily determined by the jet-to-mainstream momentum-flux ratio (J) and the orifice spacing-to-duct height ratio (S/H).

In the RQL combustor the jet fluid introduced in the quick mix section accounts for up to 75% of the total flow. Since the available pressure drop is limited, injection of large mass flows through discrete orifices requires jet-to-mainstream area ratios larger than those considered when studying conventional dilution zones. In this investigation the effects of closely spaced orifices ($S/d < 2$) are compared to the conclusions of previous studies where smaller orifices were evaluated. In addition the effects of orifice shape and inlet boundary conditions are investigated.

2. Approach

Planar Lorenz/Mie scattering was used to study passive scalar mixing of jets in crossflow. Mean concentration distributions of jet mixture fraction are acquired in planes perpendicular to the crossflow direction and used to determine mixing performance. The results are in agreement with measurements made by physical probes and other optical techniques and the utility of the technique as an engineering design tool has been previously demonstrated[25].

To delineate the performance of the various configurations and flow conditions a measure of unmixedness was used that is based on a parameter developed by Danckwertz[34] to quantify temporal fluctuations:

$$U = \frac{c'^2}{\bar{c}(1-\bar{c})} \tag{1}$$

where,

$c'^2 = \frac{1}{n}\frac{1}{m}\sum_{j=1}^{n}\sum_{i=1}^{m}(c_{ij} - \bar{c})^2$ = concentration variance

n = number of images in data set

m = number of pixels in each image

c_{ij} = instantaneous concentration at a pixel

$\bar{c} = \frac{1}{n}\frac{1}{m}\sum_{j=1}^{n}\sum_{i=1}^{m} c_{ij}$ = concentration mean = fully mixed concentration

$\bar{c}(1-\bar{c})$ = maximum concentration variance = 0.188 for a jet-mainstream flow split of 3:1

Normalization by $\bar{c}(1-\bar{c})$ allows comparison of systems of different $\bar{c}$ (different MR) and bounds U between 0 and 1. U = 0 corresponds to a perfectly mixed system, and U = 1 a perfectly segregated system.

The objective of this investigation was to screen a variety of flow and geometric configurations and compare the experimental results to similar numerical studies. Therefore, the suitability of using an unmixedness parameter based on the mean distribution alone was studied. It was found that U obtained from an ensemble of instantaneous distributions was approximately equal to that obtained from the average distribution[24]. Therefore, the unmixedness parameter used in this investigation is <u>spatial unmixedness</u> :

$$U_s = \frac{c_{var}}{c_{avg}(1-c_{avg})} \tag{2}$$

where,

$c_{var} = \frac{1}{m}\sum_{i=1}^{m}(\bar{c_i} - c_{avg})^2$ = spatial concentration variance

$\bar{c_i}$ = time-average concentration at a pixel

c_{avg} = fully mixed concentration downstream of the trailing edge of the orifice $= \bar{c}$

The measured relative light intensities are converted to measurements of concentration by normalizing so that $\frac{1}{m}\sum_{i=1}^{m}\bar{c}_i = c_{avg}$, (the metered, i.e. fully mixed value). Therefore, although $c_{avg} = \bar{c}$, the actual value of $\bar{c}$ is not measured directly and cannot be computed in the same way upstream of the trailing edge of the orifice since not all of the jet mass has been injected. Eq. 1 is still valid upstream of the trailing edge if concentration is measured directly or determined by calibration using a supplemental technique.

3. Experimental

3.1 Apparatus

Figure 3.1-1 is a schematic representation of the apparatus. The apparatus consisted of 3 parallel contiguous ducts of rectangular cross section, simulating a sector of an annular combustor. Sector width was 12 inches. The inner duct height was 2 inches for this study. The outer ducts (shrouds), which supply the injectant gas, were 1 inch in height. These were separated from the inner duct by removable, 0.12 inch thick flat plates. The injectant was fed from the shrouds to the inner duct through orifices of various sizes and shapes that were machined into the plates. Mass flow to each of the 3 ducts was controlled independently using venturi flowmeters. The maximum variation in the mean approach velocity of the mainstream flow was 6% with a turbulence level of 1.3%.

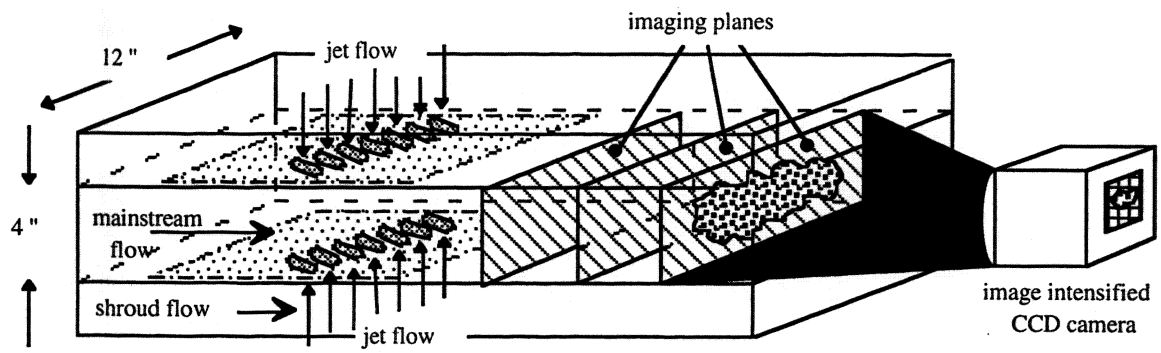

Figure 3.1-1: Experimental Configuration used to Measure Planar Concentration Distributions

3.2 Data Acquisition

Planar digital imaging was used to optically measure concentration distributions in planes perpendicular to the duct axis beginning at the trailing-edge of the orifice. The Mie scattering technique is applied by marking the jet flow with an oil aerosol (μm sized particles). A light sheet (0.02 inch thick) is created using a 2W argon-ion laser and a rotating mirror. The flow field is illuminated by passing the light sheet through a window in the side wall of the test section. An image intensified thermo-electrically cooled CCD camera, located inside the duct 2.5 ft downstream of the orifice centerline, is focused on the illuminated plane (end-on view). The camera is programmed to make exposures coincident with the sweep of the beam through the flow field. The image is digitized at a spatial resolution of 0.02 x 0.02 inch/pixel in a 576 x 100 pixel format and sent to a computer for storage. The scattered light intensity is proportional to the number of particles in the measurement volume. If only one of two streams is marked, the light intensity of the undiluted marked fluid represents mole fraction unity. For a more detailed discussion of the technique see Vranos, Liscinsky, True and Holdeman[33].

To obtain absolute mole fraction, the true mole fraction must be known at at least one point in the measurement plane. If undiluted jet fluid is present in the section sampled, then the measured distributions are absolute mole fractions. This is generally not the case, so measured distributions are relative. For some cases the digital image (light signal) was converted to mole fraction by calibration.

A trace amount of methane was introduced into the jet flow as a marker. Methane concentration, measured with an on-line hydrocarbon analyzer, provided absolute mole fraction at the sampling location. This measurement allowed conversion of the scattered light intensity distribution to mole fraction (which can then be converted to mass fraction, if desired). For those frames where gas sampling was not available, the calibration was achieved by assuming that the average intensity of the distribution across the duct was directly proportional to the fully mixed mole fraction (metered MR).

4. Results and Discussion

4.1 Review of Previous Work (Concept 1 Configurations)

Previously reported experiments under NAS3 - 25952, Task 2 clearly indicated that mixing performance is primarily a function of jet penetration. In that study the mixing of round hole and 45deg slanted slot configurations were investigated, however a parametric investigation to determine the optimimum performance of each configuration was not done. The variables that strongly affected penetration, and therefore performance, were found to be jet-to-mainstream momentum-flux ratio (J), orifice spacing (S). However, it is important to remember that performance ranking can only be done after a configuration is optimized.

For example, in Fig. 4.1-1 the concentration distributions downstream of opposed rows of slots on staggered centerlines show that slot angle relative to the mainstream flow direction drastically effects jet penetration. On the left the axially aligned slots clearly penetrated to the opposite wall, while on the right the 45 deg slanted slots penetrated to the duct centerline. A direct comparison of unmixedness of these configurations indicates that the slanted slots have better performance. But since neither configuration was optimized a general conclusion about aligned vs. slanted slots is unwarranted. The only valid conclusion is for the exact conditions that were tested.

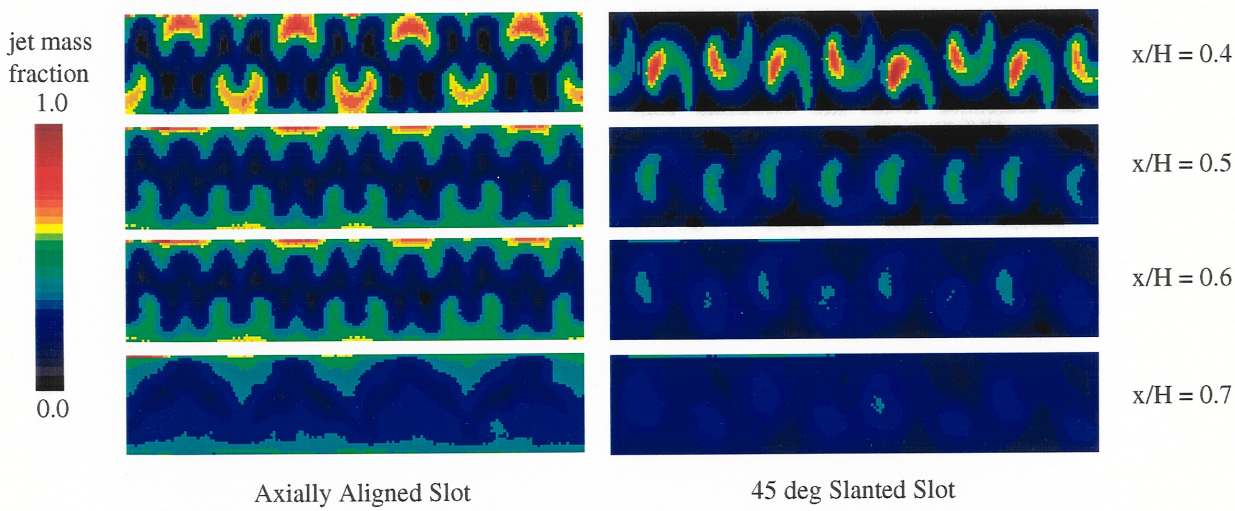

Figure 4.1-1: Concentration Distributions of Opposed Rows of Slots on Staggered Centerlines (slot aspect ratio = 4:1, J = 25, S/H = 1.0, MR = 0.38)

A second conclusion from this 1992 study was that at a given J there is an optimum orifice spacing in agreement with Holdeman[16] who has shown, on the basis of mean temperature distributions, that for multi-source injection from equally spaced round orifices in rows, mixing can be correlated by a single variable composed of the product of orifice spacing and the square root of the momentum-flux ratio, independent of orifice size. Optimum penetration and mixing for any given configuration is obtained when the square root of the momentum-flux ratio and orifice spacing are inversely proportional so that:

$$C = (S/H)\sqrt{J} \qquad (3)$$

where,

S = spacing between adjacent orifice corresponding points of adjacent orifices
H = duct height
J = momentum-flux ratio
C = 2.5 for single side injection
= 1.25 for 2-sided opposed inline injection
= 5.0 for 2-sided opposed staggered injection

4.2 Concept 2 Configurations

Round hole configurations were again studied in the second set of experiments with particular emphasis on close spacing ($S/d < 2$). In these the tests optimum configurations were identified for inline and staggered arrangements of round orifices at two momentum-flux ratios. Based on these results the suitability of Eq. 3 ($C = (S/H)\sqrt{J}$) as a design tool was evaluated.

Table 4.2-1 identifies 8 orifice plate configurations that were tested. The configurations consisted of round holes with d = 0.5, 0.75, and 0.85 and a rectangular slot with a 2:1 aspect ratio. Injection was 2-sided with the center-points of the orifices on opposite sides either directly inline, or staggered (top wall orifice center-points bisect the space between adjacent orifices on the bottom wall, i.e. the area ratios of the inline and staggered configurations were equivalent). Discharge coefficients were determined for each orifice plate configuration by measuring the ΔP across the plate over a range of mass flows and averaging. For the round orifices C_d was found to be range from 0.64 to 0.66, while plate #12 had a C_d of 0.75 Data was obtained at momentum-flux ratios of 25 and 50.

(For reference, $J = (MR)^2 / ((\rho_j/\rho_m)(C_d)^2(A_j/A_m)^2)$

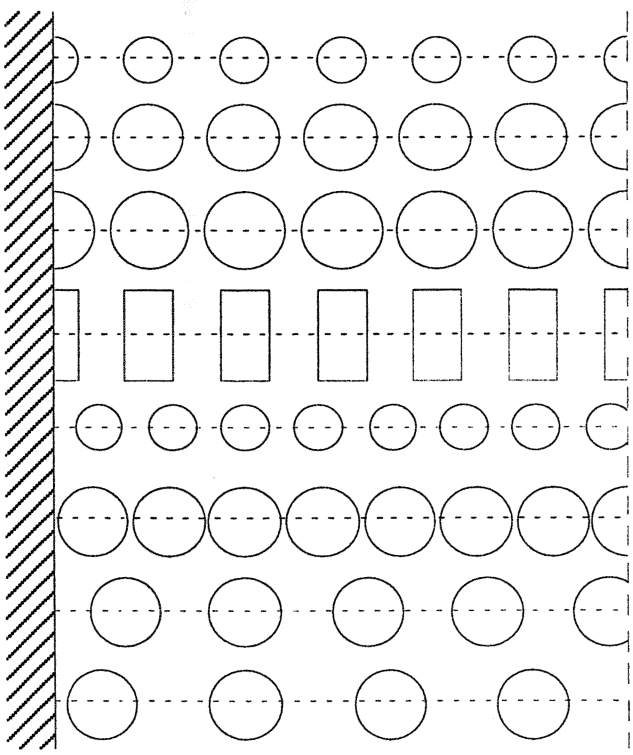

Plate #	d (in)	S/H	S/d	Aj/Am	Trailing* Edge	Blockage†
10	0.50	0.50	2.0	0.20	0.250	0.50
2	0.75	0.50	1.3	0.44	0.375	0.75
11	0.85	0.50	1.2	0.57	0.425	0.85
12	(0.5 x 1.0)	0.50	1.2	0.57	0.425	0.85
1	0.50	0.38	1.5	0.26	0.250	0.67
9	0.75	0.40	1.1	0.55	0.375	0.94
7	0.75	0.63	1.7	0.35	0.375	0.60
3	0.75	0.75	2.0	0.29	0.375	0.50

Table 4.2-1: Concept 2 Orifice Plate Configurations

* x projection / H (H = 2 inches for all tests)

† y projection / S (blockage = the reciprocal of S/d for the orifice configurations in Table 4.2-1)

4.2.1 Orifice Spacing

Mean concentration distributions for two-sided injection from opposing rows of round holes with the top and bottom hole centered opposite each other (inline) are shown in Fig. 4.2-1 at x/H = 0.375 and 0.500 when J = 25. A 10-level color scale is used to represent contours of jet mass fraction from 0 to 1.0 (pure mainstream fluid colored red = 0 and pure jet fluid colored black = 1.0). In each figure the orifice spacing decreases from S/H = 0.75 in the top row to S/H = 0.4 in the bottom row. Hole diameter is constant at 0.75 inches, consequently A_j/A_m for plate #9 (bottom row) is about 50% larger than plate #3 (top row). Therefore the mass flow ratio also increases from the top row to the bottom row in Fig. 4.2-1. The fully mixed concentration, C_{avg}, i.e. the color corresponding to the fully mixed condition, is not the same contour for all of the configurations shown in Fig. 4.2-1.

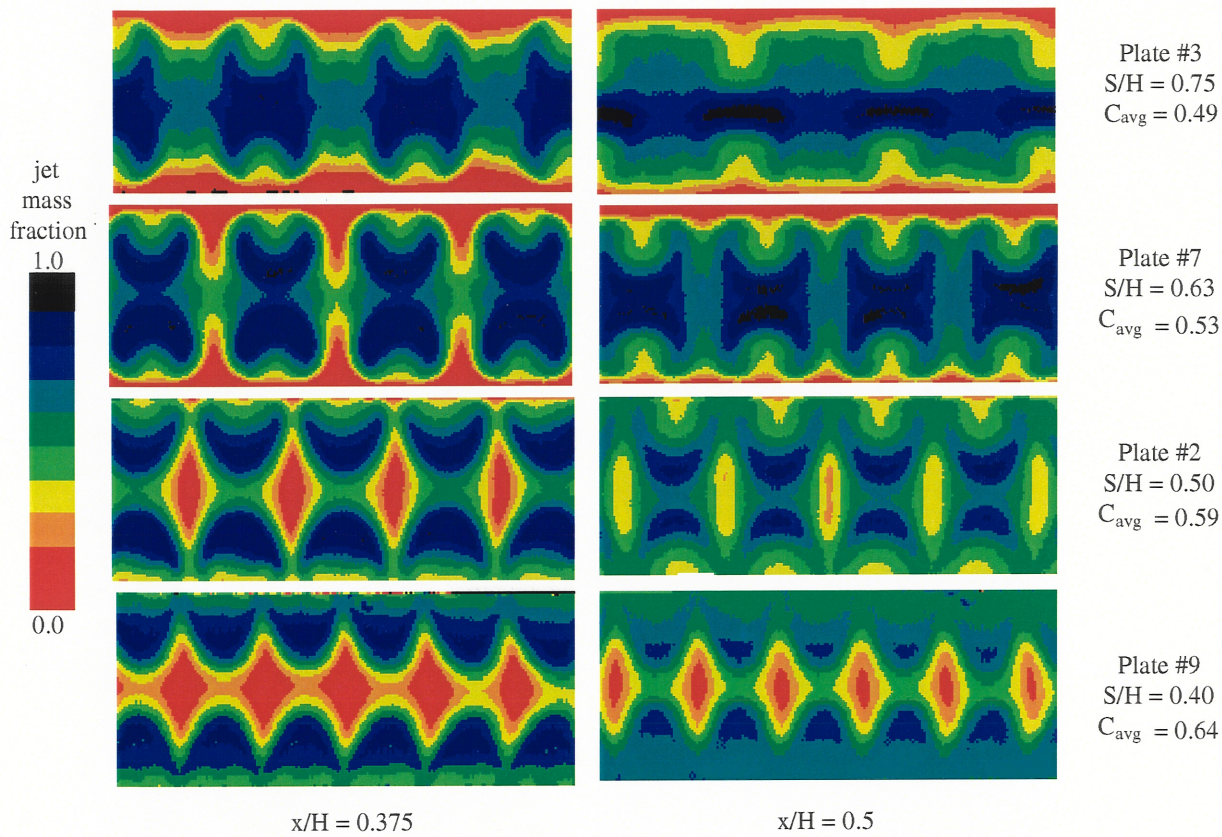

Figure 4.2-1: Average Concentration Distributions for Opposed Inline Round Holes d=0.75" and J = 25

From Fig. 4.2-1 the effect of orifice spacing on jet penetration is clear: at a given J, jet penetration decreases as spacing decreases. At S/H = 0.75 the jet trajectories from the top and bottom walls collide at the mid-point of the duct, while at S/H = 0.4 the jets remain near the walls of the duct . The optimum appears to be nearest to an S/H of 0.5.

In previous studies by Holdeman[3] jet penetration and centerplane profiles were found to be independent of orifice diameter, when S/H and $\sqrt{J}$ were inversely proportional (Eq. 3). An optimum S/H of 0.25 would be predicted using Eq. 3 for opposed inline orifices (C = 1.25) and J = 25. However it should be noted that in Ref. 3 the "optimum" was obtained by visual inspection of the centerplane profiles and therefore depends on x/H and what one perceives as "optimum" depends on the downstream distance.

In Fig. 4.2-2 the effect of S/H on mixing effectiveness is shown in a plot of U_S vs. downstream distance for the same configurations shown previously in Fig. 4.2-1. An optimum spacing is indicated at S/H = 0.5, which corresponds to a jet penetration between the case where the jets "over-penetrate" at S/H = 0.75 (top row in Fig. 4.2-1) and "under-penetrate" at S/H = 0.4 (bottom row in Fig. 4.2-1). The orifice configuration shown as plate #2 in Table 1 provided the fastest mixing at J = 25.

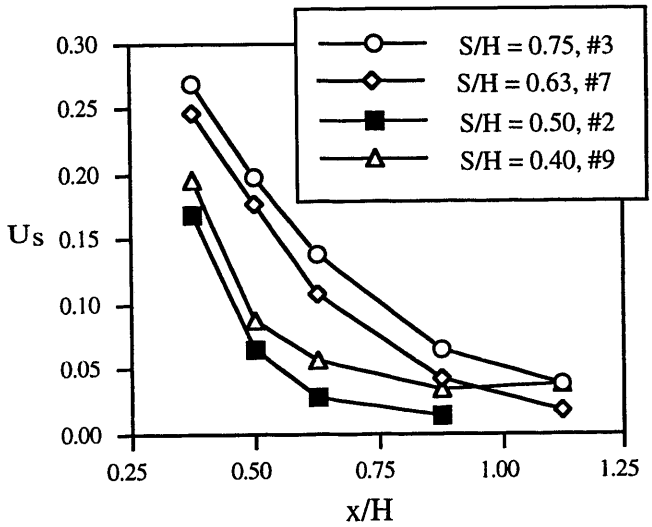

Figure 4.2-2: Effect of S/H on Spatial Unmixedness for Inline Round Holes d = 0.75" and J = 25

Eq. 3 is evaluated in Fig. 4.2-3 at J = 25 for the fastest mixing configuration at d = 0.75 (#2, shown previously in Fig. 4.2-2) and two configurations with d = 0.50 and similar values for C. Mixing was most effective for each hole size when C = 2.5. The unmixedness curves for both plates #2 and #10 (Table 4.2-1) at J = 25 support Eq. 3 in that mixing rate is a function of spacing and J, but independent of orifice diameter.

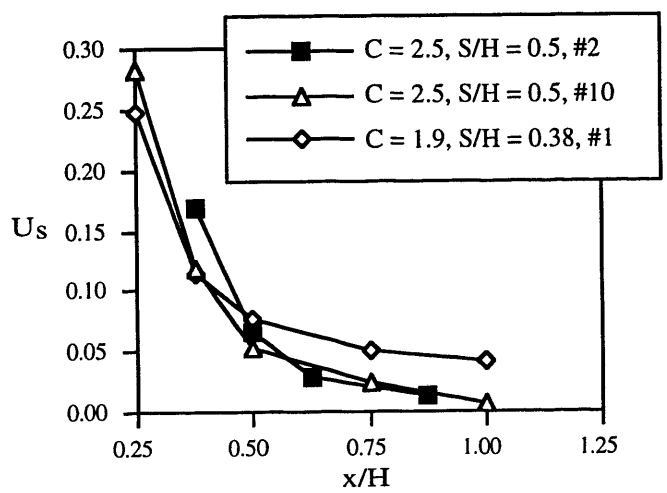

Figure 4.2-3: Effect of Orifice Diameter on Spatial Unmixedness at J = 25 for Opposed Inline Round Holes

U_S is plotted as a function of x/H at J = 50 in Fig. 4.2-4. The values of U_S are lower at J = 50 than at J = 25 (Figs. 4.2-2 and 4.2-3) indicating that mixing effectiveness has increased with increased J. The best mixing was provided by orifice plate # 1 (Table 4.2-1) which has an S/H = 0.38, consistent with Eq. 3, i.e. higher values of J require smaller values of S. The corresponding value for C was 2.7 vs. the value of 2.5 found for J = 25.

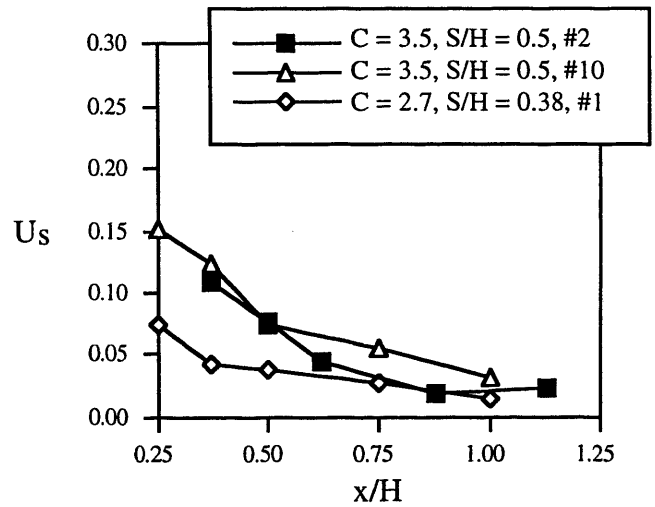

Figure 4.2-4: Effect of Orifice Diameter on Spatial Unmixedness at J = 50

The value of 2.5 obtained for C for opposed rows of inline orifices is higher than the value of 1.25 found by Holdeman. It is suspected that two factors influence the variation in C: (1) data analysis in previous studies compared centerplane profiles, while this study measures the nonuniformity of the entire duct cross section, and (2) the orifice configurations of this study are outside of the range of the previous data set, i.e. previous $A_j/A_m < 0.1$ and $S/d \geq 2$ (widely spaced) while in this study $A_j/A_m > 0.2$ and $S/d < 2$ (closely spaced). Also, note that the current results are consistent with CFD[3].

4.2.2 Orifice Diameter and Blockage

Eq. 3 can be used as a design tool, given J, to specify the optimum spacing, S, for a row of inline round holes. However, apparently for durability reasons, it may be necessary to consider the trade-off between blockage (B)(webb between adjacent orifices) and longer injection length (rectangular slots). In the limit, a 2D slot is obtained which has been shown to be a poor mixer compared to a row of discrete orifices[23]. This would suggest that in addition to an optimum S, B is also an important consideration. Unfortunately, for round holes, B and d cannot be tested independently. A comparison of orifice plates #10, #2, and #11 affords an evaluation progressively greater B, while maintaining a constant S.

In Fig. 4.2-5 U_S is plotted as a function of x/H at J= 25 for B = 0.50, 0.75 and 0.85. Note that for these configurations blockage = d since S = 1. In addition since C = 2.5, the configurations are optimized at this J. The unmixedness curves for the three configurations are similar, which indicates that B ranging from 0.50 to 0.85 does not affect mixing rate. Even a relatively high blockage still allows the mainstream flow to squeeze between the jets and generate a 3D flowfield. However, the level of U_S in the near-field (x/H < 0.5) is influenced by d. At x/H < 0.5, the lowest levels of U_S are obtained for the smallest diameter holes. Although optimum spacing as specified by Eq. 3 does not appear to be a function

of d (same value of C is obtained independent of d), the level of U_S at a particular value of x/H is affected by the axial length of the orifice, i.e. the mixing curves shift downstream along with the trailing edge of the orifice. Fig. 4.2-5 indicates that the lowest values of U_S are obtained in a minimum x/H when the axial length of the orifice is minimized.

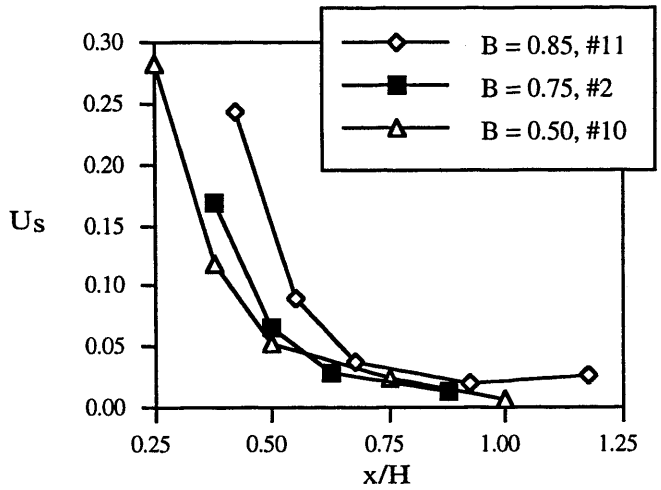

Figure 4.2-5: Effect of Blockage on Spatial Unmixedness at J = 25 for Opposed Inline Round Holes at S/H = 0.5

In Fig. 4.2-6 U_S is shown as a function of x/H at J = 25 for a rectangular slot with a 2:1 aspect ratio (plate #12, Table 4.2-1) and a round hole with d = 0.85 (plate #11, Table 4.2-1). The area ratios of the two configurations are equilvalent. Mixing rates of the two configurations are not the same. The levels of unmixedness are significantly higher for the slot configuration and the rate is slower. Fig. 4.2-6 further emphasizes that mixing effectiveness diminishes as axial length of injection increases. However, the problem of liner durability could be addressed by the use of rectangular slots if slot length ≈ hole diameter.

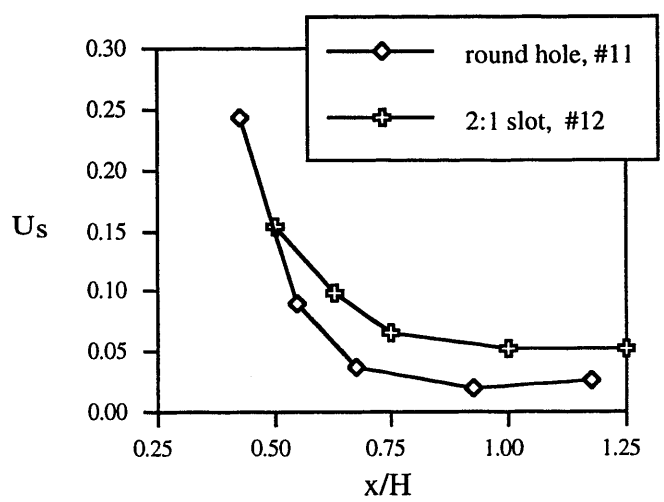

Figure 4.2-6: Comparison of Equal Area Equal S Opposed Inline Round Holes and Rectangular Slots at J = 25

4.2.3 Inline vs. Staggered

Opposed jet configurations are not limited to inline orientations. In Fig. 4.2-7 two examples of inline and staggered configurations are shown at J = 50 for round holes. Both configurations are for holes with d = 0.75, but the case on the left has an S = 1.0 (S/H = 0.5) and the one on the right an S = 1.5 (S/H = 0.75). Note that A_j/A_m (and therefore MR) for the inline and staggered configurations are equivalent at each S/H. When S/H = 0.50 (plate #2), the inline and staggered distributions are very similar: the jets penetrate to the center of the duct and appear to remain relatively unmixed at x/H = 0.625 (left-hand column). In contrast, at S/H = 0.75 (plate #3) the inline and staggered distributions are quite different (right-hand column). The staggered configuration appears better mixed at x/H = 0.625. The staggered jets become elongated as they pass by each other. An interaction of the counter-rotating vortex pair from the top and bottom jets is indicated by the loss of the characteristic "horseshoe" shape in the near-field. It appears that the resulting vortex system is less stable than any of the other three configurations. Note that the jet fluid apparent nearest the walls in the lower right figure (S/H = 0.75, staggered) is from jets injected from the opposite wall, whereas the jet fluid nearest the walls in the other figures is from jets injected from the adjacent wall.

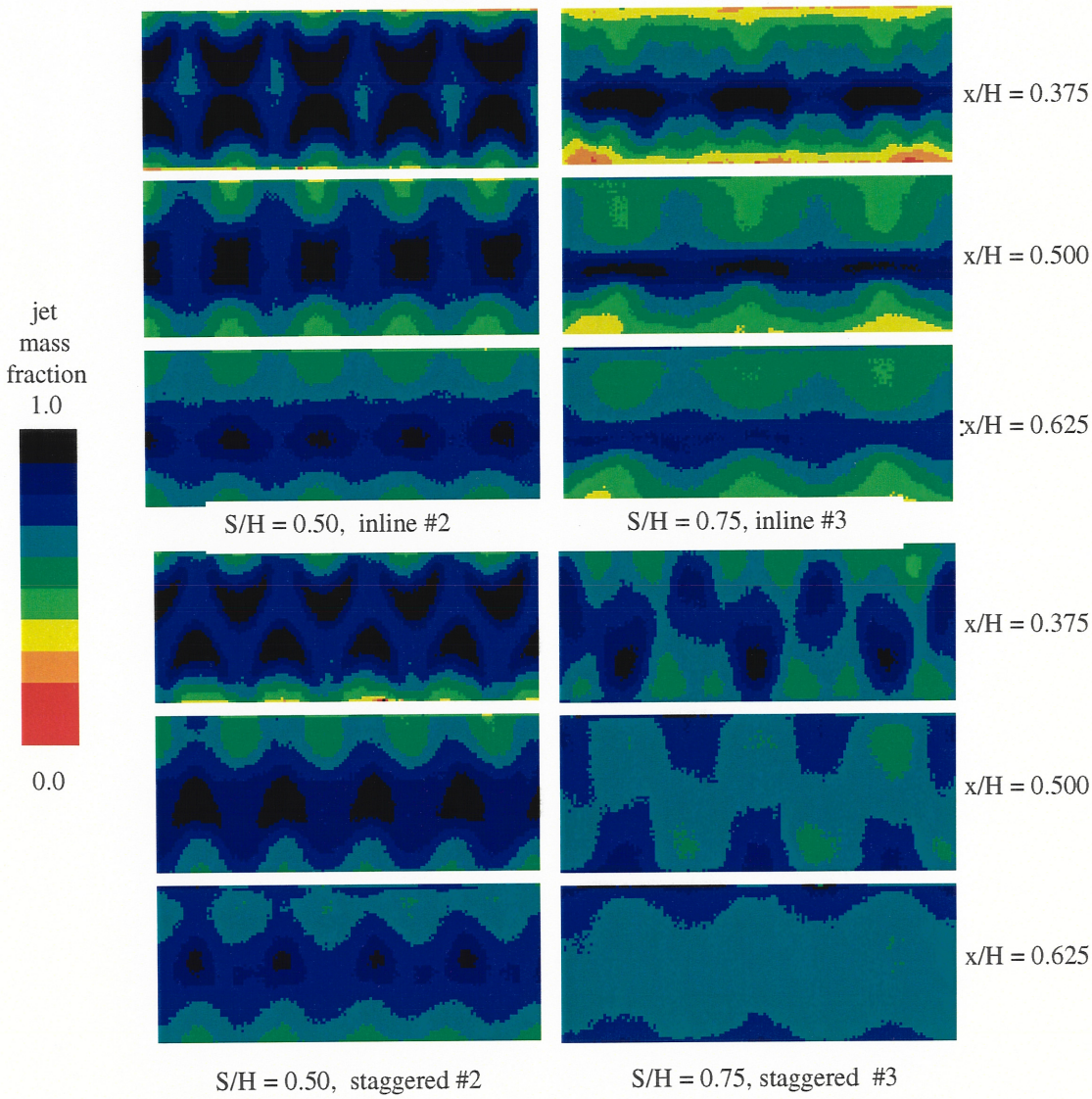

Figure 4.2-7: Comparison of Staggered and Inline Orientations at J = 50
(see configurations in Table 4.2-1)

In Fig. 4.2-8 U_s is plotted as a function of x/H for the four configurations in Fig. 4.2-7. As predicted the staggered configuration is the most effective mixer. A systematic inspection of staggered configurations for the plates shown in Table 4.2-1 indicated that the staggered orientation does not increase mixing effectiveness until $S/d \geq 2$. The implication is that there may also be an optimum S/d, in addition to an optimum S/H, for staggered configurations. If the required A_j/A_m can be achieved with $S/d \geq 2$, it appears that staggering may produce lower levels of U_s in the near-field if J is sufficient for the jets from opposite walls to penetrate past eachother.

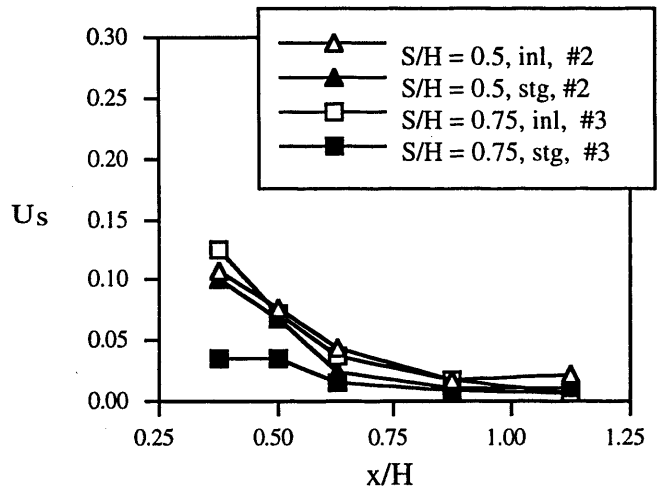

Figure 4.2-8: Effect of Orifice Orientation on Spatial Unmixedness at J = 50

4.3 Concept 3 Configurations

The effect of orifice shape was investigated in a third set of experiments. In these tests the configurations were not optimized to allow ranking based on performance. The effect of orifice shape on the jet mixture fraction distribution was evaluated for 2-sided injection at J = 25. Table 4.3-1 identifies 5 orifice plate configurations that were compared to a round hole configuration (plate #3). Discharge coefficients were assumed to be 0.65 for all tests.

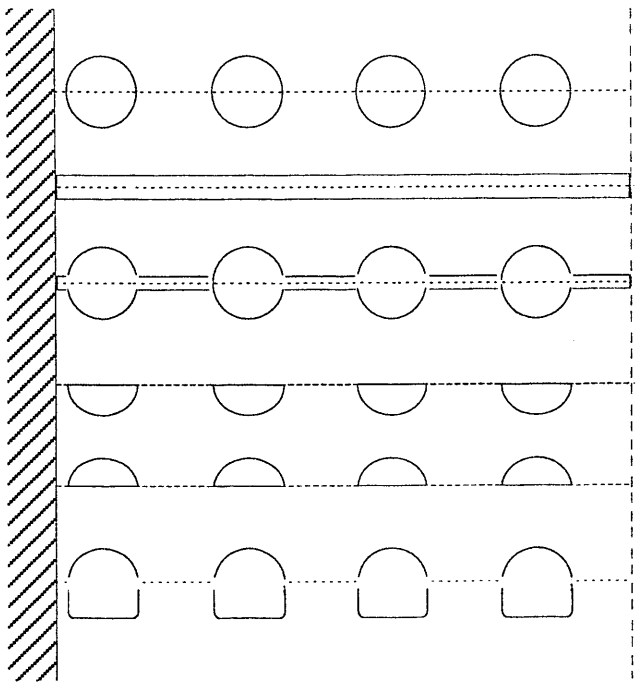

Plate #	d (in)	S/H	S/d	Aj/Am	Trailing* Edge	Blockage†
3	0.75	0.75	2.00	0.29	0.375	0.50
5	-----	-----	-----	0.25	0.125	1.00
4	(0.75)	(0.75)	(2.00)	0.36	0.375	0.50
6	-----	0.75	(2.00)	0.15	0.188	0.50
6	-----	0.75	(2.00)	0.15	0.188	0.50
8	-----	0.75	(2.00)	0.32	0.375	0.50

Table 4.3-1: Concept 3 Orifice Plate Configurations

* x projection / H (H = 2 inches for all tests)
† y projection / S (blockage = the reciprocal of S/d for the orifice configurations in Table 4.3-1)

Concentration distributions as a function of downstream position for the 6 orifice configurations are shown in Fig. 4.3-1. Slightly different penetration is observed for each configuration, however the distributions are similar enough to speculate that none of the tested shapes would significantly augment mixing relative to the baseline round hole if optimized configurations were compared.

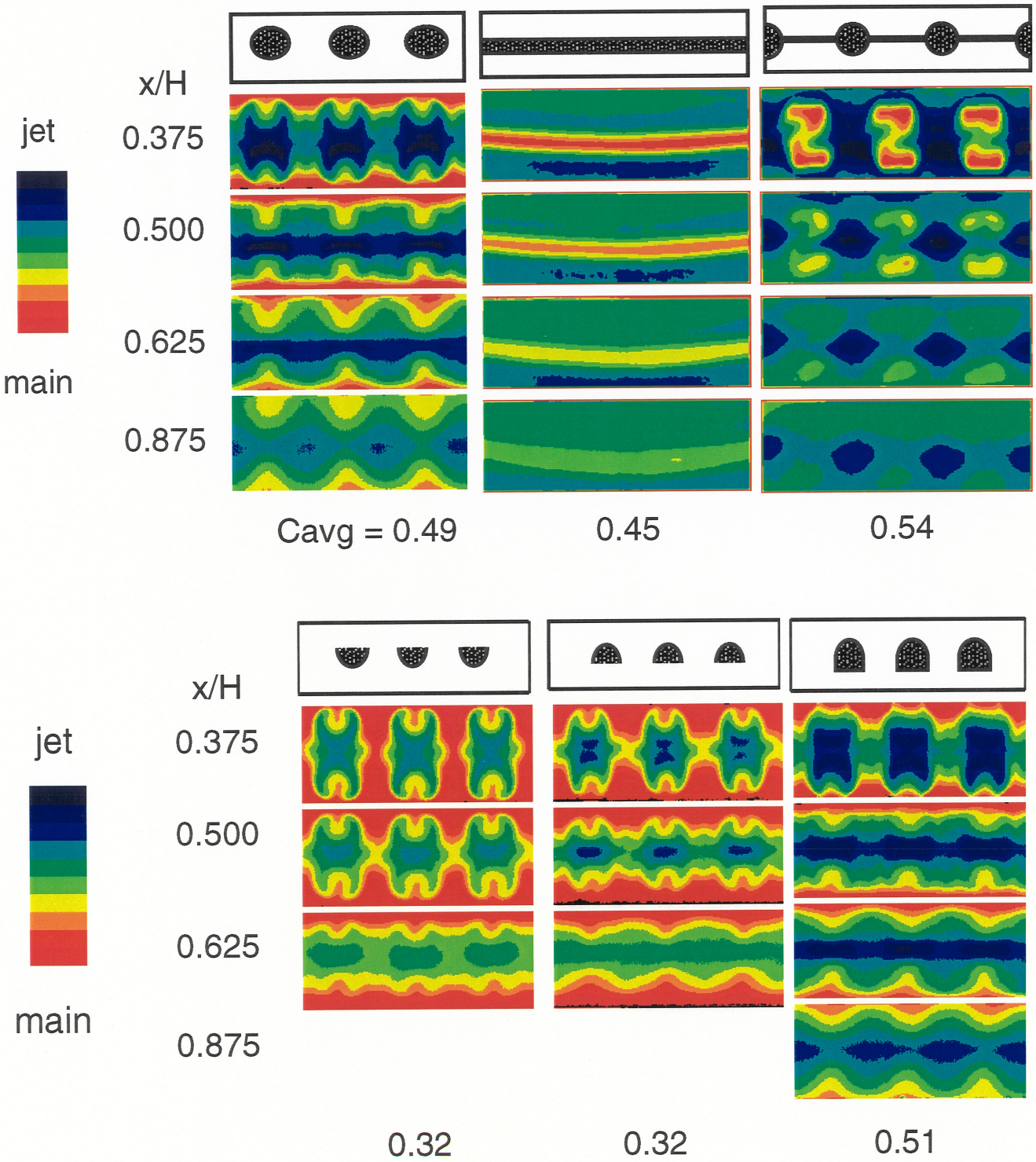

Figure 4.3-1: Concentration distributions for the orifice configurations shown in Table 4.3-1 (J = 25)

4.4 Effects of Initial Conditions

In order to demonstrate how "ideal" mixing results relate to hardware constraints several variations in inlet flow boundary conditions were studied.

4.4.1 Approach Profile

The mainstream velocity profile was modified as shown in Fig. 4.4-1 to provide two different approach flow conditions. The inline orifice configuration that was tested used plate #3 in Table 4.3-1. The tests were performed at J = 25 which gave overpenetration for the uniform approach profile. As indicated in the concentration distributions in Fig. 4.4-2 the result of the symmetrical approach profile was increased jet penetration relative to the baseline at x/H = 0.375, whereas the skewed approach profile reduced penetration from of top jets and increased penetration of the bottom jets, again relative to the uniform approach profile.

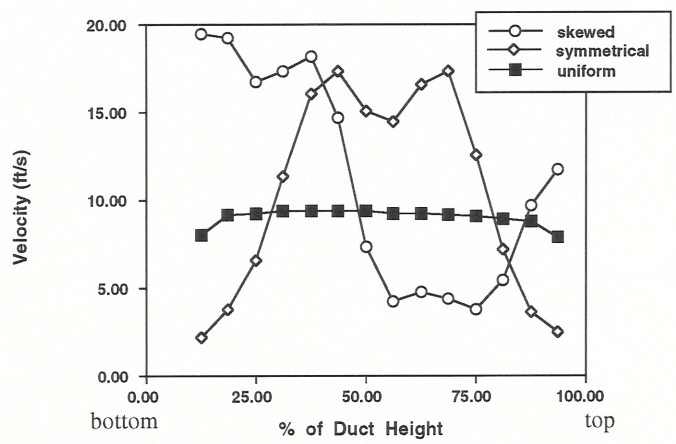

Figure 4.4-1: Approach Velocity Profiles

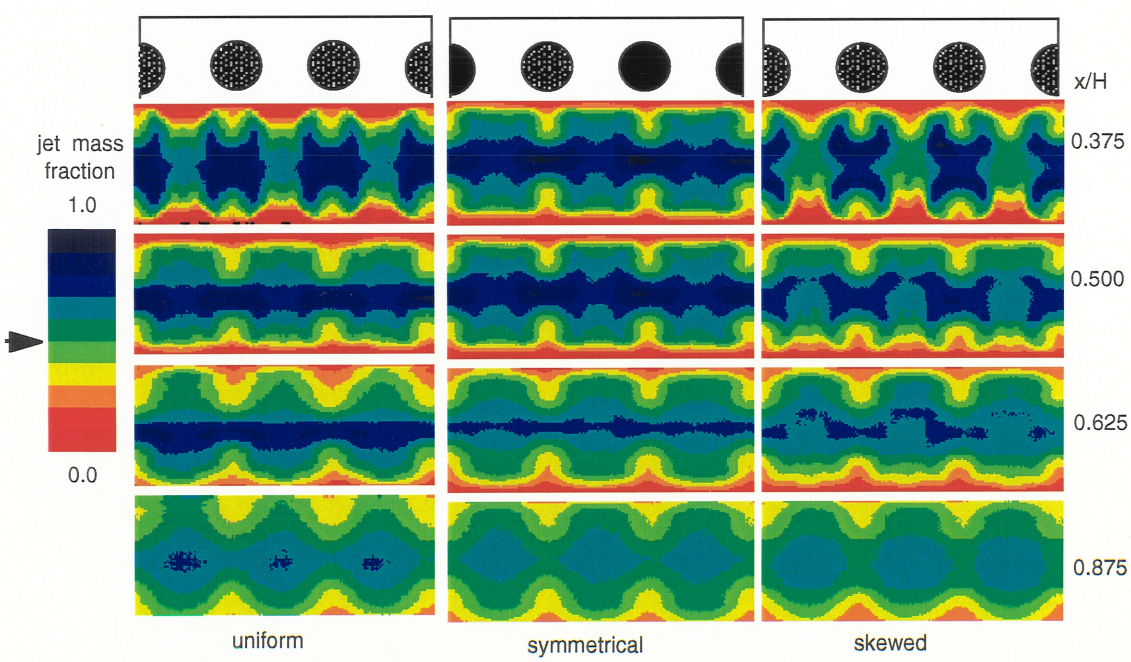

Figure 4.4-2: Concentration Distributions for the Tested Approach Velocity Profiles

4.4.2 Contraction of the Mainstream

The effect of the duct geometry upstream of the jet injection location was studied by testing the 6 configurations shown in Fig. 4.4-3. An optimized inline orifice configuration was used for all testing consisting of 0.74" diameter round holes spaced 0.85" on center and tested at J = 36. Concentration distributions of configuration C1, C3, and C6 are compared to the baseline geometry in Fig. 4.4-4a - c (concentration distributions for C2, C4, and C5 are not shown). Jet profiles are less symmetrical for C1, C3 and C6 and the net result is enough of a decrease in jet penetration to decrease mixing performance as indicated by the umixedness plot shown in Fig. 4.4-5

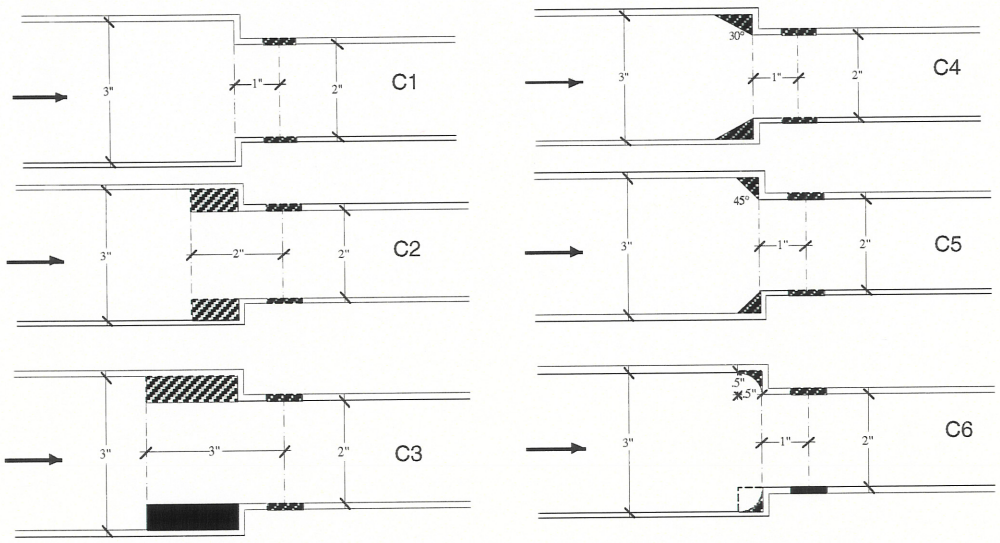

Figure 4.4-3: Configurations to Study the Effect of Mainstream Approach Geometry

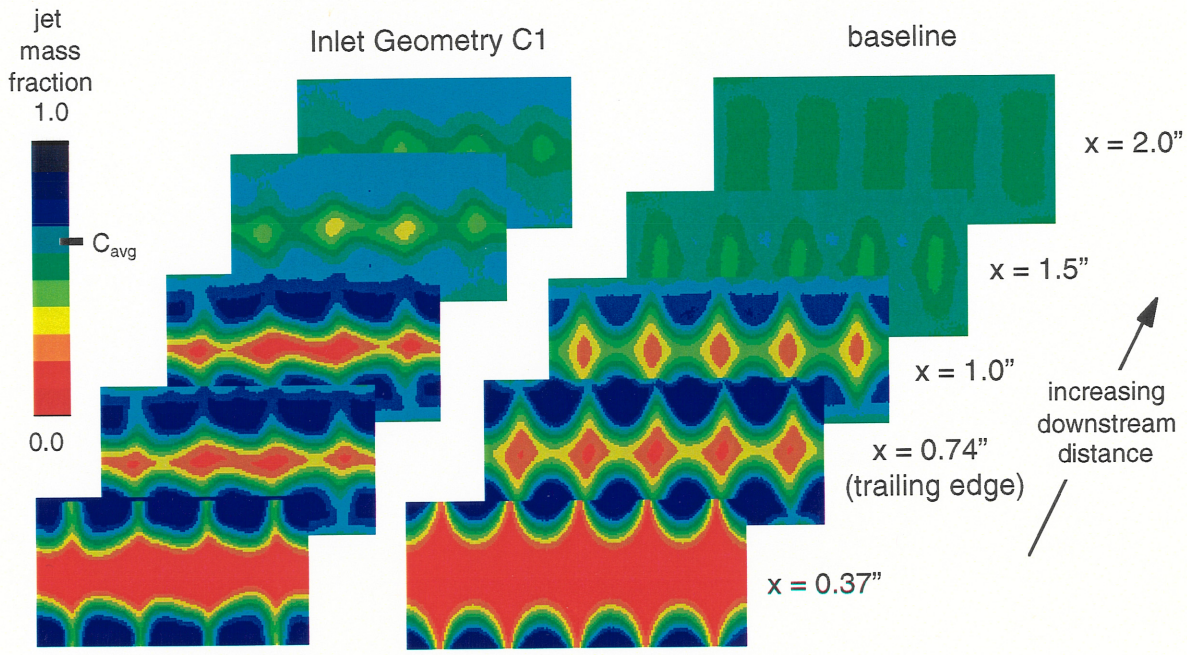

Figure 4.4-4a: Comparison of Concentration Distributions for Inlet Geometry C1 and the Baseline (d = 0.74, S/H = 0.425, J = 36)

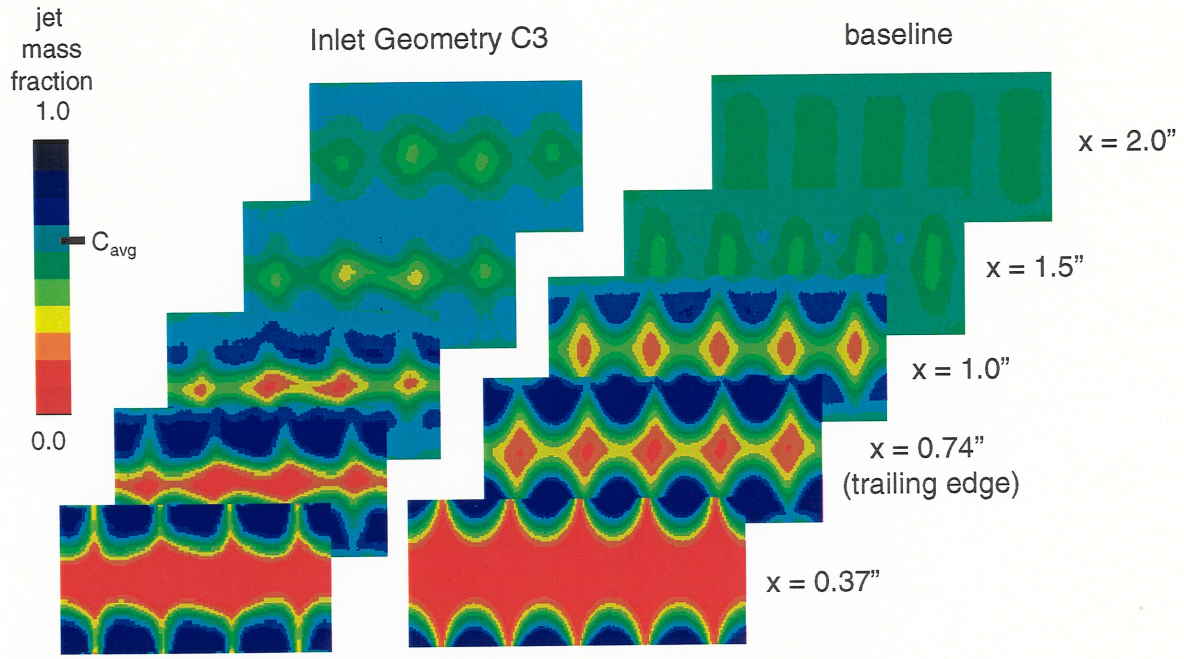

Figure 4.4-4b: Comparison of Concentration Distributions for Inlet Geometry C3 and the Baseline (d = 0.74, S/H = 0.425, J = 36)

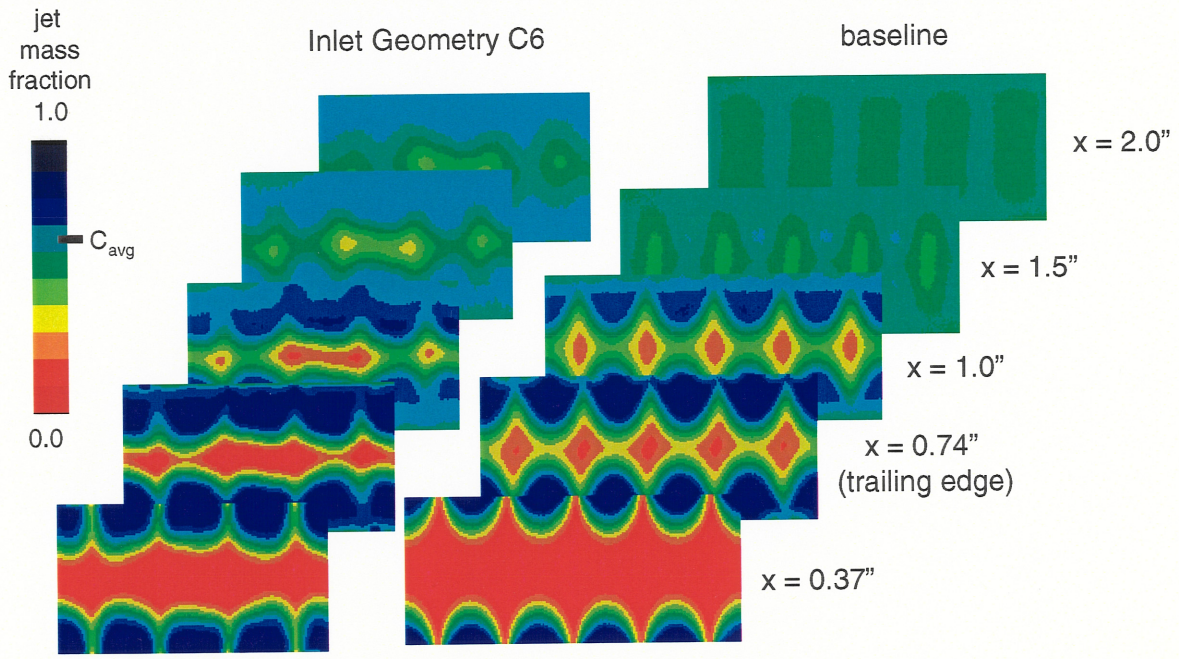

Figure 4.4-4c: Comparison of Concentration Distributions for Inlet Geometry C6 and the Baseline (d = 0.74, S/H = 0.425, J = 36)

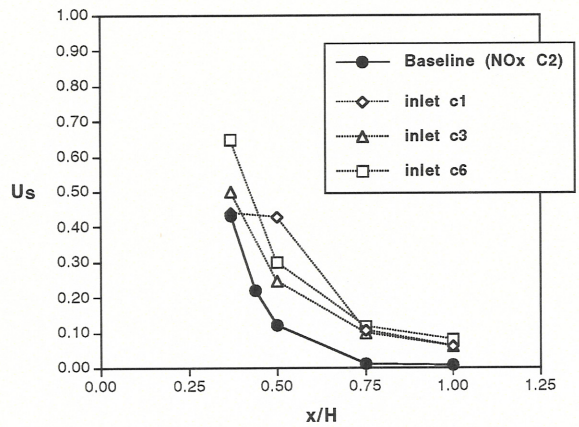

Figure 4.4-5: Comparison of Spatial Unmixedness

4.4.3 Jet Delivery System

As a practical hardware issue it is desireable to introduce the mixing air using a curved delivery system shown schematically on the left-hand side of Fig. 4.4-6. On the right-hand side of the figure the pressure distribution at the points indicated on the grid are plotted. The results indicate flow separation at the curve resulting in a jet exit profile that is depressed at the mid-point relative to the orifice edge. Concentration distributions from the curved jet delivery system are compared to the baseline (plenum) case in Fig. 4.4-7. Jet penetration decreases due to the flow separation and performance is poor.

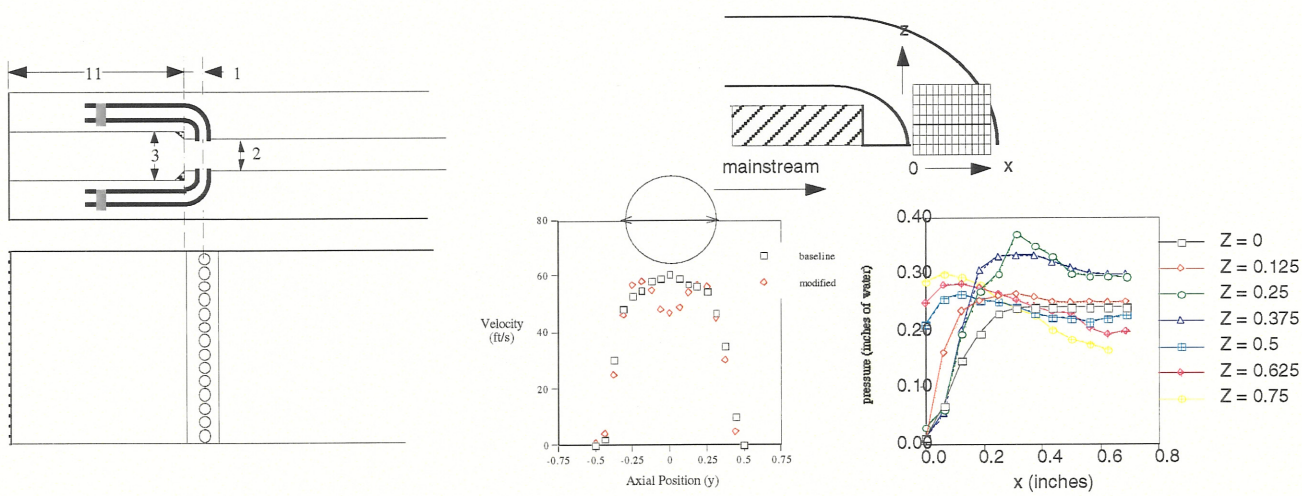

Figure 4.4-6: Schematic of the Curved Jet Delivery System and Pressure Distribution at the Discharge

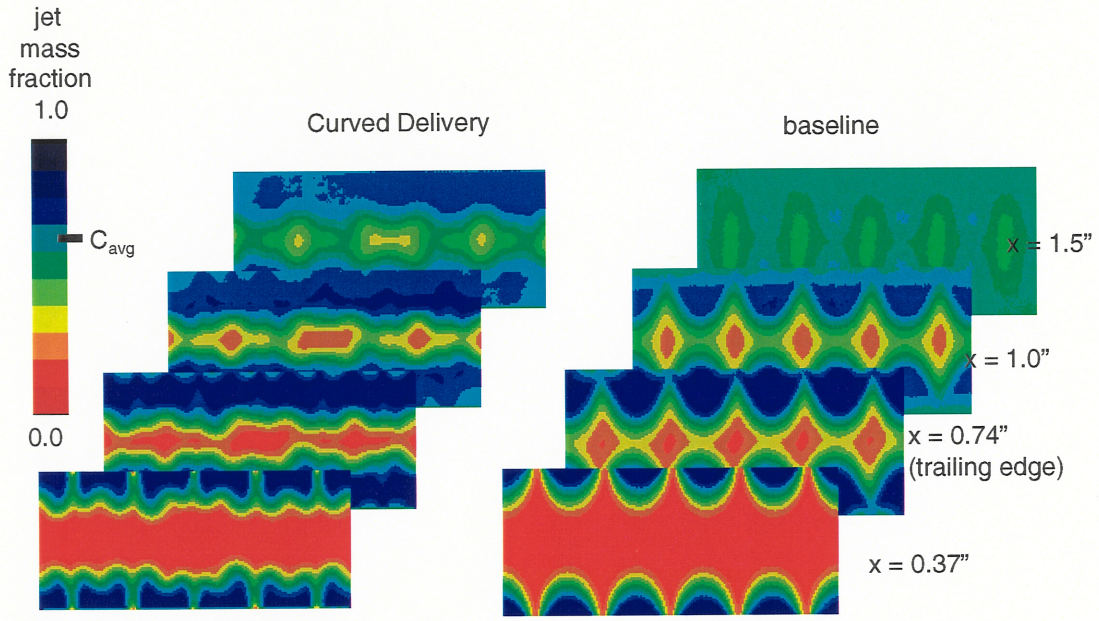

Figure 4.4-7 Concentation Distribution Comparison of Curved and Straight Delivery Systems

4.4.4 Upstream Swirl

The effect of upstream swirl was investigated by using the 4-swirler bulkhead shown in Fig. 4.4-8. The bulkhead was placed 3" upstream of the jet injection location. An optimized inline orifice configuration consisting of 0.74" diameter round holes spaced 0.85" on center and a mass flow ratio corresponding to a J of 36 was used (all of the mainstream mass flow was forced through the swirlers). The resulting concentration distribution is shown in Fig. 4.4-9. The imprint of the swirlers is indicated by three regions of relatively unmixed mainstream fluid at x/H = 1.14" and the skewed penetration of the jets.

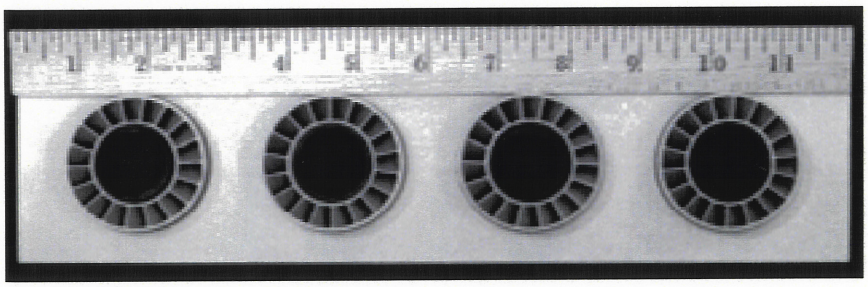

Figure 4.4-8: End-on View of Bulkhead containing 4 Swirlers

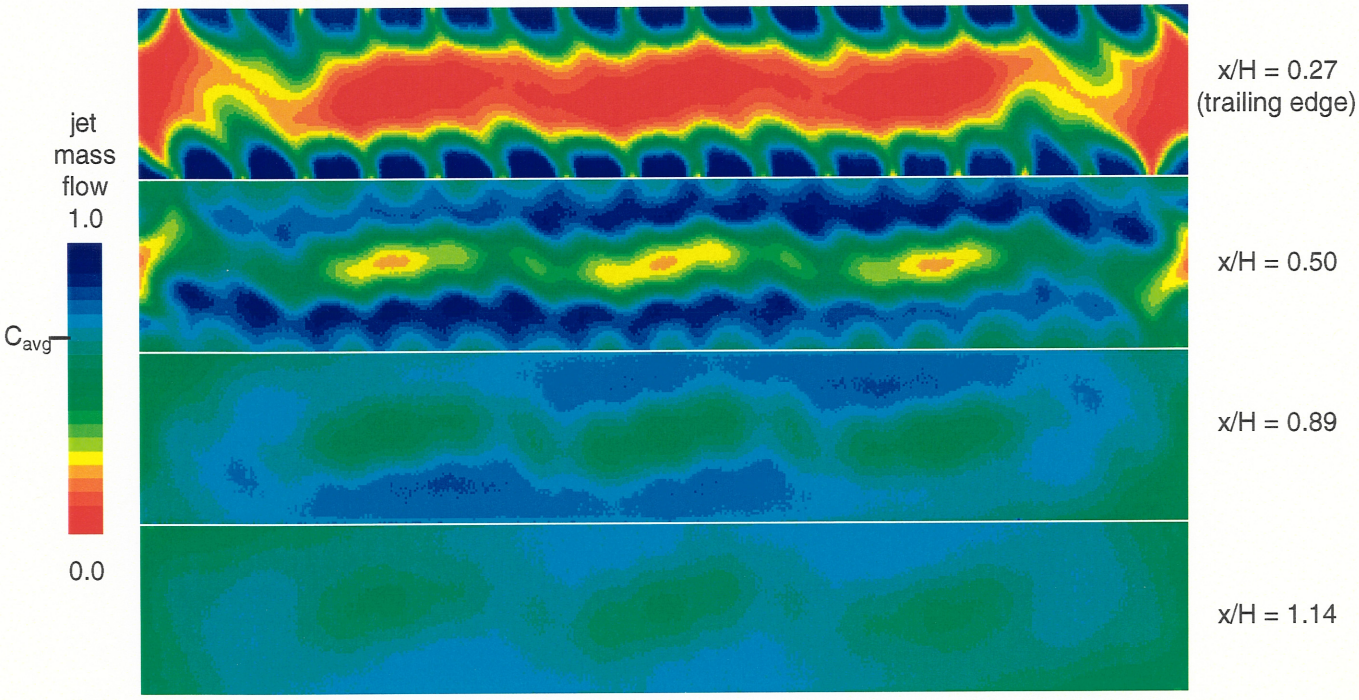

Figure 4.4-9: Concentration Distribution

4.5 Blockage Revisited

The general inverse relationship of J and S/H (Eq. 3) has been shown to apply when extended to RQL conditions of MR = 2 and S/d ≤ 2. However at those conditions, the proportionality constant, C, has been found, both experimenally and numerically, to be ≈2.5, compared to a value of 1.25 which was reported at S/d ≥ 2. To determine whether C is a function of orifice width, a set of "optimized" orifices with varying geometric blockages (B) were investigated. Rectangularly shaped orifices were used in order to maintain MR = 2.0 and S/H = 0.425 for all configurations. (Blockage cannot be varied at constant MR and S/H using circular orifices).

The effect of varying blockage from 0.59 to 1.0 was investigated by testing the 7 orifice plate configurations shown in Table 4.5-1. The first 6 configurations were designed to be optimum inline mixing configurations based on the results of a numerical parametric investigation of aspect ratio and orifice spacing by Bain, Smith and Holdeman[5]. In that numerical study, aspect ratio and orifice shape were found to have little effect on the mixing performance of inline configurations when a value of 2.55 was used for C in Eq. 3. The plates were designed for a MR of 2.0 when J = 36 and S/H = 0.425 in order to compare with those numerical results. However, the experimentally measured C_d for the plates was significantly less than the design point C_d. The lower C_d required J = 48 to achieve MR = 2.

Plate #	Aspect Ratio	Configuration	Width x Length (Δy" x Δx")	Area Ratio (Aj / Am)	Design Cd (*)	Blockage†
1	1-to-1.5	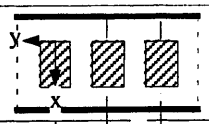	0.502 x 0.752	0.444	0.75 (0.66)	0.59
2	1-to-1.25	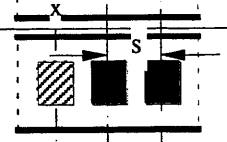	0.550 x 0.687	0.444	0.75 (0.64)	0.65
3	1-to-1	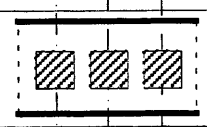	0.614 x 0.614	0.444	0.75 (0.65)	0.72
4	1-to-1.25	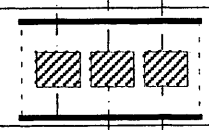	0.687 x 0.550	0.444	0.75 (0.62)	0.81
5	1-to-1.5	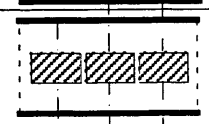	0.752 x 0.502	0.444	0.75 (0.62)	0.89
6	1-to-1	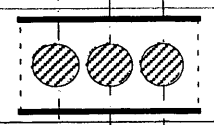	0.695 x 0.695	0.444	0.75 (0.66)	0.82
7	-----	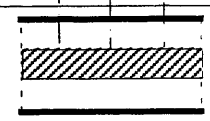	0.850 x 0.44	0.444	0.75 (0.68)	1.00

Table 4.5-1: Optimum Inline Orifice Configurations for MR = 2.0, S/H = 0.425, J = 36

* measured discharge coefficient

† y projection / S

Average jet mass fraction concentration distributions perpendicular to the mainstream flow direction for blockages of 0.59, 0.65, 0.81 and 0.89 are shown in Fig.4.5-1 at 5 downstream positions starting at the trailing edge of each row of orifices. The concentration distributions are plotted using 10 color-coded contours each representing a range in jet mass fraction of 0.1 from pure jet fluid = 1.0 (blue) to pure mainstream fluid = 0.0 (red). The fully mixed concentration of each configuration (C_{avg}) is 0.667.

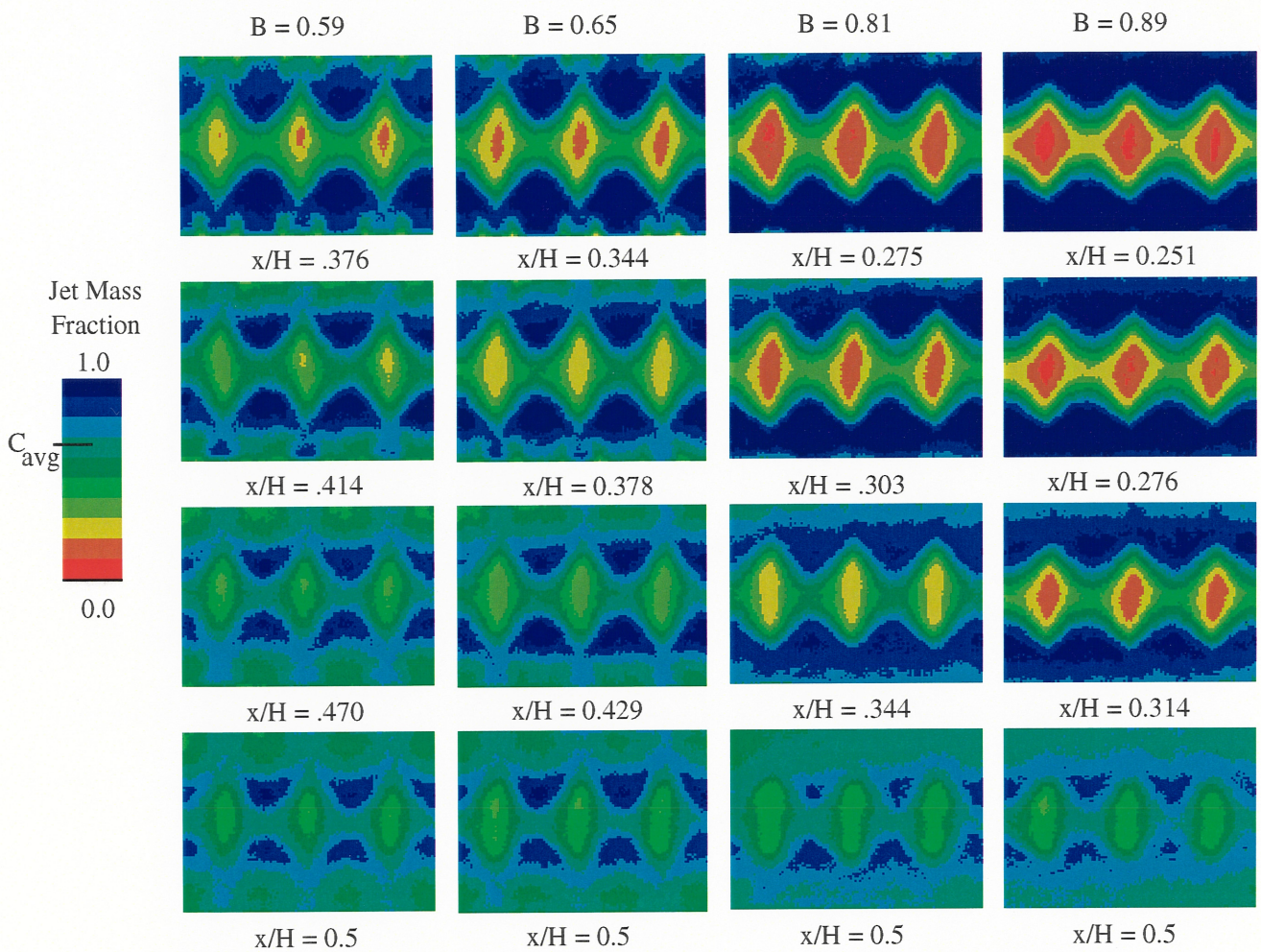

Figure 4.5-1: Effect of Blockage on Opposed Inline Orifices at MR = 2.0, S/H = 0.425, J = 48

In each configuration the jets penetrate to about 1/4 of the duct height, which has been shown to provide optimum mixing in an inline configuration[3]. As the jets move downstream (top to bottom in

fig. 4.5-1) the distributions become similar, and at x/H = 0.5 the distributions appear equivalent.

In fig. 4.5-2 average jet mass fraction concentration distributions are shown for a square (B = 0.72), a circle (B = 0.82), and a 2D slot (B = 1.0). The concentration distributions of the 2D slot indicate that the mainstream fluid remains in the center of the duct while the jet fluid stays near the walls. The mixing rate of this configuration appears lower than the cases where B < 1.0. At x/H = 0.5 the distributions of the rectangular and circular configurations appear similar to each other and to the corresponding distributions in Fig. 4.5-1.

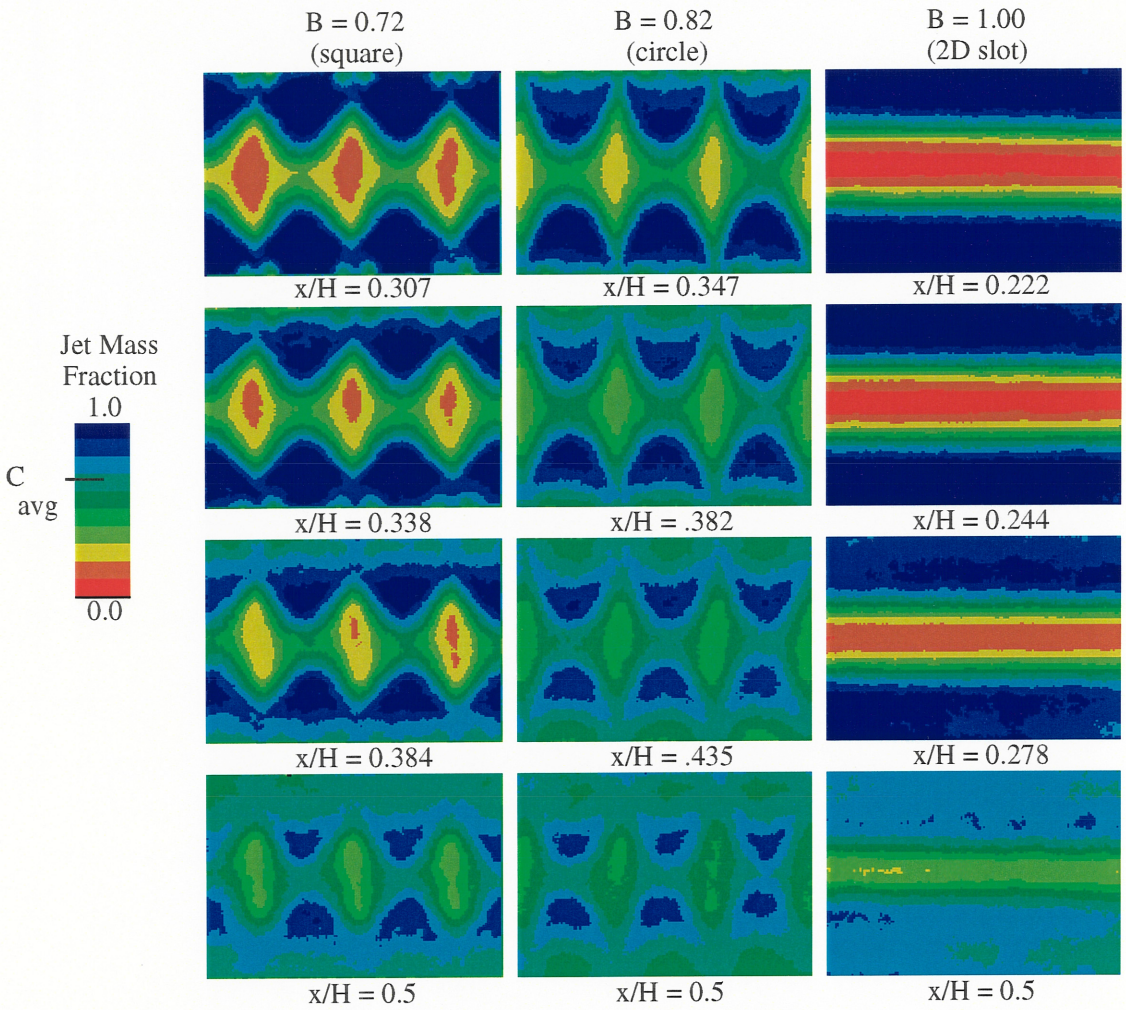

Figure 4.5-2: Effect of Blockage on Opposed Inline Orifices at MR = 2.0, S/H = 0.425, J = 48

Spatial unmixedness is plotted as a function of downstream position (x/H) for the 7 configurations in Fig. 4.5-3. The curves are similar for all configurations except the 2D slot, which is consistently less mixed as a function of x/H. The surprising result is that mixing is independent of B over a range of 0.59 to 0.89. Similar performance independent of B can probably be attributed to the fact that the effective aerodynamic blockage is significantly less than the geometric blockage because of the vena contracta of the jet. For example, plate 3 has a blockage of 0.72 based on physical dimensions, but only 0.58 when C_d is considered. Therefore even a configuration such as plate 5 that has a B of 0.89 allows a significant proportion of the mainstream to pass between adjacent jets due to the vena contracta of the orifice. The shear created by mainflow passing between the jets is necessary for development of a 3D flowfield which promotes mixing. The importance of the interplay between the jets and mainstream is evident from the concentrtation distribution of the 2D slot which confines the mainstream to the center of the duct.

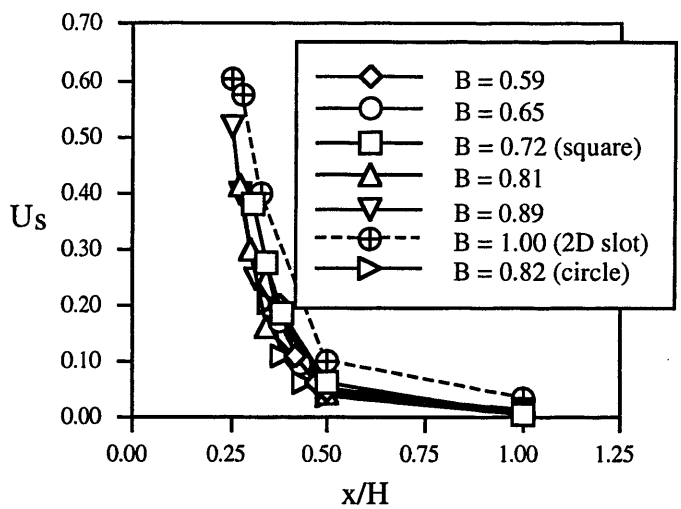

Figure 4.5-3: Effect of Blockage on Spatial Unmixedness
at MR = 2.0, S/H = 0.425, J = 48

Orifice configurations with geometric blockages ranging from 0.59 to 0.89 had similar mixing performance when compared at one-half duct height downstream of injection. Blockage was varied by changing the orifice aspect ratio from 1-to-1 to 1-to-1.5 while maintaining orifice spacing-to-duct height (S/H) at 0.425, jet-to-mainstream mass flow ratio (MR) at 2.0, and jet-to-mainstream momentum-flux ratio (J) at 48. The result indicates that the design correlating expression (at MR = 2) for optimum inline mixing of $2.5 \approx (S/H)\sqrt{J}$ is independent of the webb between adjacent orifices and therefore independent of orifice width.

As a practical design issue, the results indicate that webb thickness can be set by mechanical constraints and not aerodynamics associated with mixing performance. Eq. 3 can be used without concern for a decrease in performance due to high B. The rate of mass addition as a function of downstream distance can therefore be increased by reduction of webb thickness so that the axial length of the orifice can be minimized. Furthermore, circular and rectangularly shaped orifices with aspect ratios between 1-to-1 and 1-to-1.5 in both bluff and aligned orientations have similar levels of U_s at

4.6 NOx Inference Data Sets

In collaboration with CFDRC a set of data was acquired to be used in conjunction with a software tool developed by CFDRC to infer emissions from cold flow data. The 4 configurations shown in Table 4.6-1 were selected. They consist of 2 optimum cases and an overpenetration and an underpenetration case based on Eqn. 3. Mass flow ratio was constant at 2.0. Configuration 1 of Table 4.6-1 is shown schematically on the left-hand side of Fig. 4.6-1 with the location of the 10 data planes shown on the right side. Selected data planes of concentration distributions for the 4 configurations are shown in Figs. 4.6-2 to 4.6-5.

In the CFDRC NO_X inference code the isothermal jet mixture fractions were used as input. The 10 experimental planes were then interpolated to 100 computational planes. For each of these planes the local temperature and species concentration were determined from local jet mixture fraction assuming equilibrium chemistry. NO formation was then computed based on the Zeldovich mechanism. For details of the procedure see Ref. 4.

Config #	Orifice Width (in)	Orifice Length (in)	Spacing (in)	J		S/H	Webb (in)	B	MR	C
1	0.65	0.65	0.85	36		0.425	0.2	0.76	1.97	2.55
4	0.725	0.91	0.85	15		0.425	0.125	0.85	1.98	1.65
		Orifice Diameter (in)	Spacing (in)	J		S/H	Webb (in)	B	MR	C
2		0.74	0.85	36		0.425	0.11	0.87	2.00	2.55
3		0.625	0.85	70		0.425	0.225	0.74	1.99	3.56

Table 4.6-1: NO_x Inference Data Sets

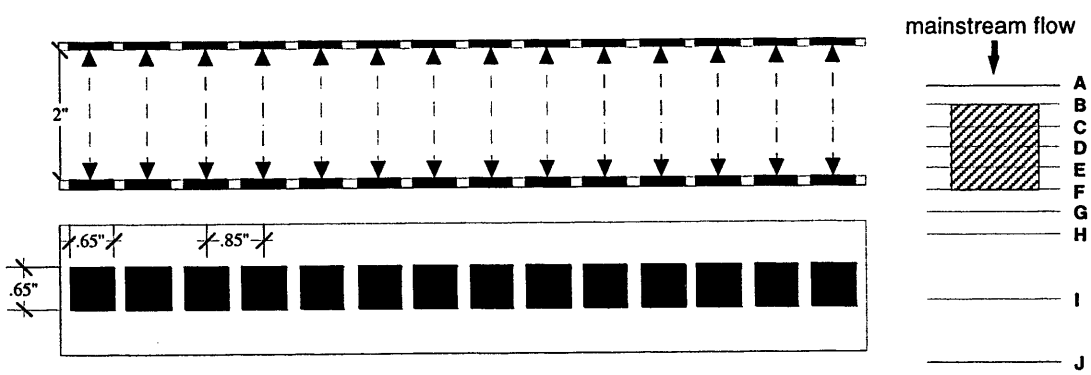

Figure 4.6-1: Schematic of Configuration 1 and Data Plane Locations

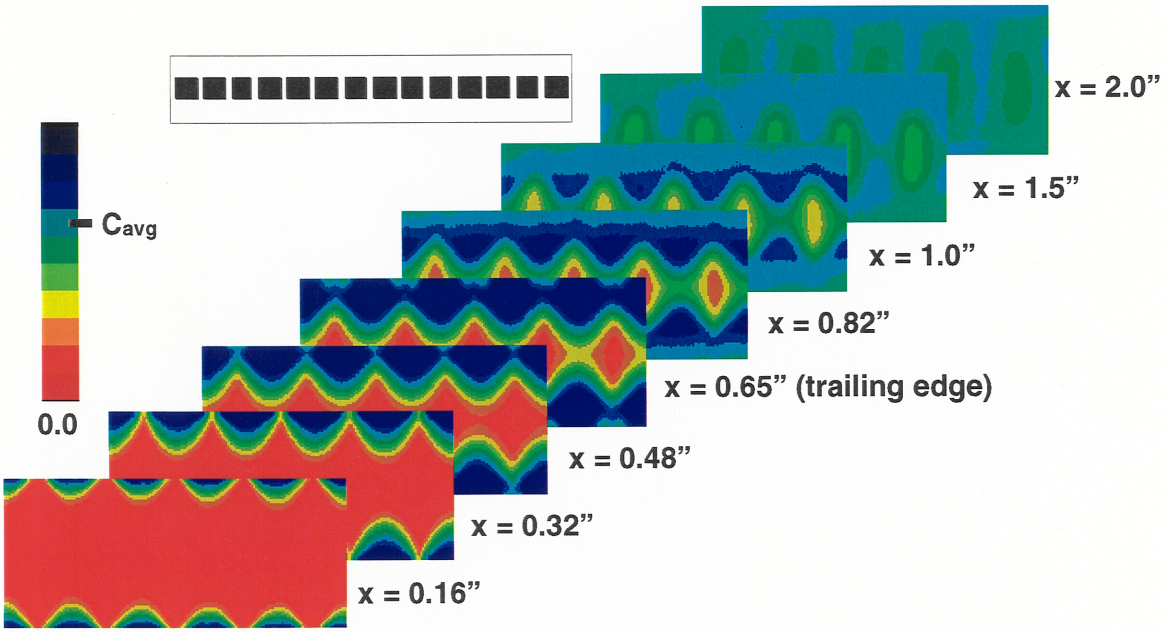

Figure 4.6-2: Concentration Distributions for Configuration 1
(0.65 square, J = 36, S/H = 0.425)

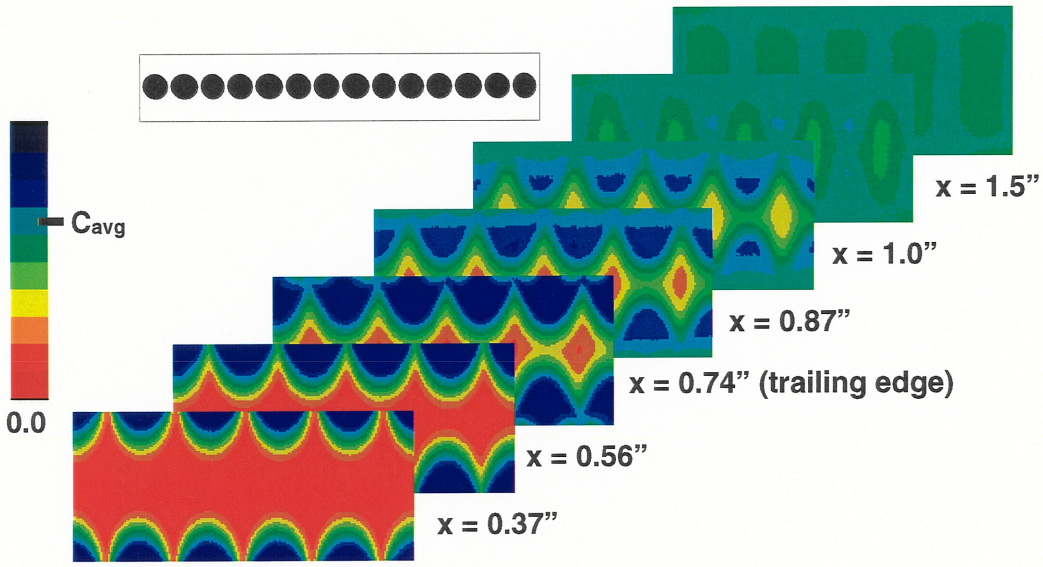

Figure 4.6-3: Concentration Distributions for Configuration 2
(0.74 circle, J = 36, S/H = 0.425)

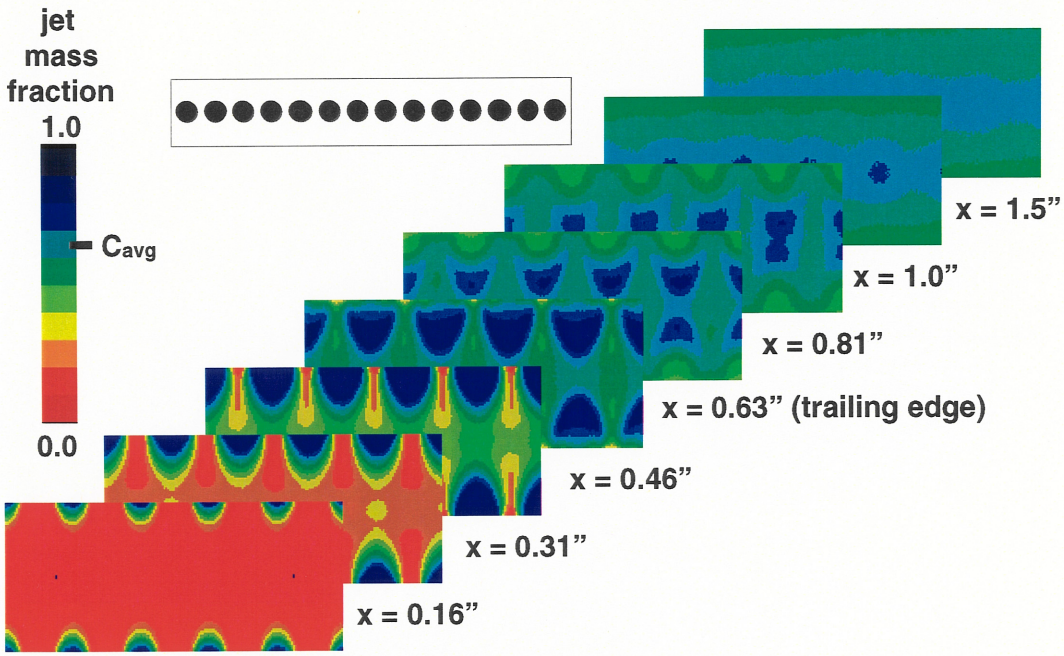

Figure 4.6-4: Concentration Distributions for Configuration 3
(0.625 circle, J = 70, S/H = 0.425)

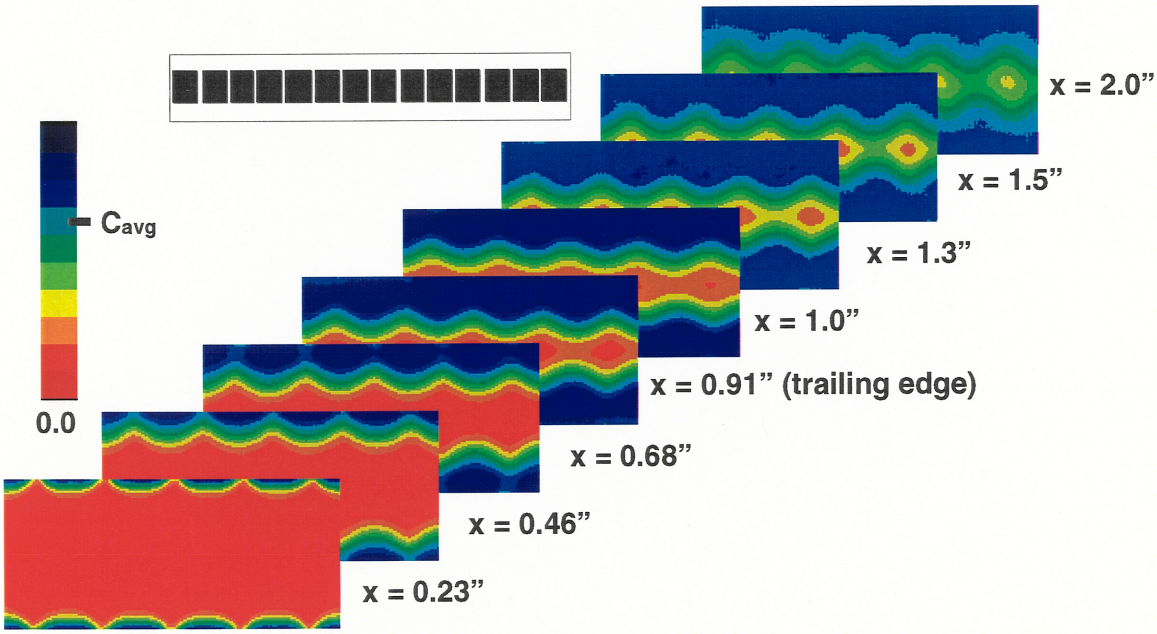

Figure 4.6-5: Concentration Distributions for Configuration 4
(0.725 x 0.91 rectangle, J = 15, S/H = 0.425)

x/H = 0.5, but note that the bluff orientation offers the characteristic of smaller x projection per unit area.

4.7 Non-Circular Single Jets

The use of orifice shape to passively control the mixing process has been studied in non-reacting and reacting systems, and the ability of noncircular, low-aspect-ratio orifices to augment mixing rates in these systems has been demonstrated[35-39]. The increased mixing rate is attributed to generation of "scales" which are smaller than those created by round/circular shapes. The result is increased mixing on a molecular scale which increases reaction rate. Most previous studies of noncircular orifices use nozzles to generate inlet boundary conditions with components of axial vorticity. The jet then exhausts into a quiescent surrounding. In this investigation a turbulent jet was injected perpendicular to a uniform crossflow through several different types of sharp-edged orifices. Jet penetration and mixing was studied using planar Mie scattering to measure time-averaged mixture fraction distributions of circular, square, elliptical, and rectangular orifices of equal geometric area injected into a constant velocity crossflow. Hot-wire anemometry was also used to measure streamwise turbulence intensity distributions at several downstream planes.

The mixing experiments were performed in a 12 cm x 12 cm horizontal windtunnel with provision for jet injection through one wall as shown in Fig. 4.7-1. The air for the crossflow was supplied by a blower attached to the tunnel inlet with a 20 cm diameter flexible duct. The inlet/settling section was 43 cm x 43 cm and contained a dense "furnace" filter to distribute the flow, followed by a honeycomb and a series of 2 wire-mesh 50% open screens for flow conditioning. The 43 cm x 43 cm cross section then contracted on all four sides by a 3rd order polynomial to the 12 cm x 12 cm test section. The crossflow/mainstream velocity was set at 6.6 m/s and velocity variation across the test section was less

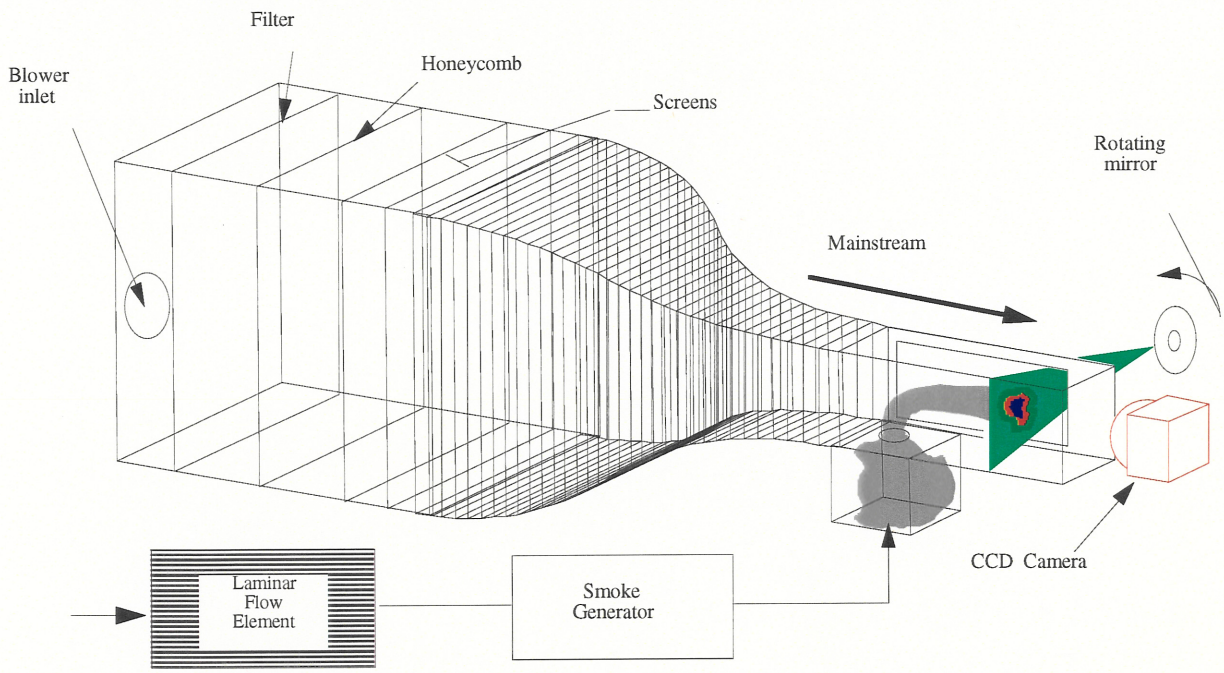

than 5%. Turbulence intensity was 1%.

Figure 4.7-1: Experimental Configuration used to Measure Planar Concentration Distributions

The jet enters the tunnel through a sharp-edged (3.2 mm thick) orifice machined into an interchangeable bottom wall. The other three walls of the test section are 3.2 mm thick plate glass. The jet flow originates in a 10 cm x 10 cm x 12 cm plenum attached to the bottom of the test section. The mass flow into the plenum was maintained at 0.0043 kg/s using a laminar flow element.

Table 4.7-1 identifies the 6 orifice configurations that were tested. Note that configuration C & D and E & F are the same orifice shape rotated 90 deg. The physical area of each orifice was 2.86 cm^2. Discharge coefficients (C_d) were measured in a separate apparatus for each orifice plate at the mass flow rate used in the investigation. The C_d of each plate was found to be 0.67 resulting in a bulk jet velocity of 19 m/s. The jet-to-mainstream momentum-flux ratio (J) was therefore 8.2. This J was chosen so that the jets would have a trajectory that roughly followed the centerpoint of the tunnel and avoid wall contact. The Reynolds number of the jet was typically 24000.

Configuration	Orifice Shape	Width x Length (cm x cm)	Aspect Ratio	Angle
A	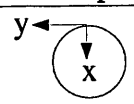	1.91 x 1.91	1 : 1	0
B		1.69 x 1.69	1 : 1	0
C		1.35 x 2.70	2 : 1	0
D		2.70 x 1.35	2 : 1	90
E	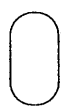	1.27 x 2.54	2 : 1	0
F		2.54 x 1.27	2 : 1	90

Table 4.7-1: Sharp-edge Orifice Configurations

Mie scattering was the primary diagnostic used to optically measure jet mixture fraction distributions in planes parallel and perpendicular to the duct axis. The planar digital imaging technique (see Ref. 33) is applied by marking the jet flow with an oil aerosol (μm size particles). A light sheet (0.5 mm thick) is created using a 2W argon-ion laser and a rotating mirror. The flow field was illuminated to acquire planes oriented in either: (1) a side view, by passing the light sheet through the orifice centerline in the axial direction, or (2) the end-on view, by passing the light sheet through planes perpendicular to the injection wall (y-z plane) at various axial locations. An image-intensified thermo-

electrically cooled CCD camera fitted with standard 35mm lenses was used to record the scattered light intensity. For the side views the camera was focussed through the side window on the illuminated plane. For the end-on view the camera was located inside the duct 61 cm downstream of the orifice centerpoint. The camera was programmed to make exposures coincident with the sweep of the beam through the flow field. The mean concentration distributions were acquired over 15 seconds and represent the time-average intensity of about 2000 instantaneous distributions which were then digitized in a 380 x 380 pixel format (pixel size = 0.3 mm x 0.3 mm x 0.5 mm) and sent to a computer for storage. The scattered light intensity is proportional to the number of particles in the measurement volume. If only one of two streams is marked (in this study the jet fluid), the light intensity of the undiluted marked fluid represents mole fraction unity.

In addition to the optical measurements, a series of gas sampling probe measurements were made to provide independent calibration of the Mie scattering distributions. A methane tracer was introduced into the jet fluid and a total hydrocarbon analyzer was used to detect the methane. For those measurements a 3.2 mm diameter stainless steel probe was mounted on a platform that could be moved both vertically and horizontally. While the downstream location (x-direction) was positioned manually, a stepper motor moved the probe in 3.2 mm increments throughout the y-z plane under computer control. A delay of 2 seconds at each station was sufficient to purge the sample line. The on-line total hydrocarbon analyzer continuously measured the methane concentration which was compared with the reference concentration to obtain jet mixture fraction at 1369 data points.

Mean flow velocity in the streamwise direction and the rms value were obtained using a linearized constant temperature hot-wire anemometer. A single wire oriented perpendicular and horizontal to the mainstream flow (y-z plane) was traversed in a fashion similar to the gas sampling probe described in the previous paragraph. Average quantities were recorded at 440 points/plane and turbulence intensity is reported. The probe orientation was not varied, therefore only velocity components in the streamwise direction were measured. Although the probe response was 13kHz, spectra were not recorded.

Mean concentration distributions for the six orifice configurations are shown in Fig. 4.7-2. The distributions are side views, the x-z plane bisecting the orifice and parallel to the mainstream flow direction. A 10-level color scale is used to represent contours of jet mass fraction from 0 to 1.0 (pure mainstream fluid colored red = 0 and pure jet fluid colored dark blue = 1.0, note that the acquired data has a resolution several orders of magnitude greater than that displayed by the contour plot). Mainstream flow is from left-to-right and the jet obviously enters from the bottom left. A plan view of the orifice shape is displayed in the upper left corner. The images are cropped so that the left side begins at x = 0, the leading edge of the orifce, and the right side is at x/d = 5.5 (where d = the diameter of an equivalent area circle).

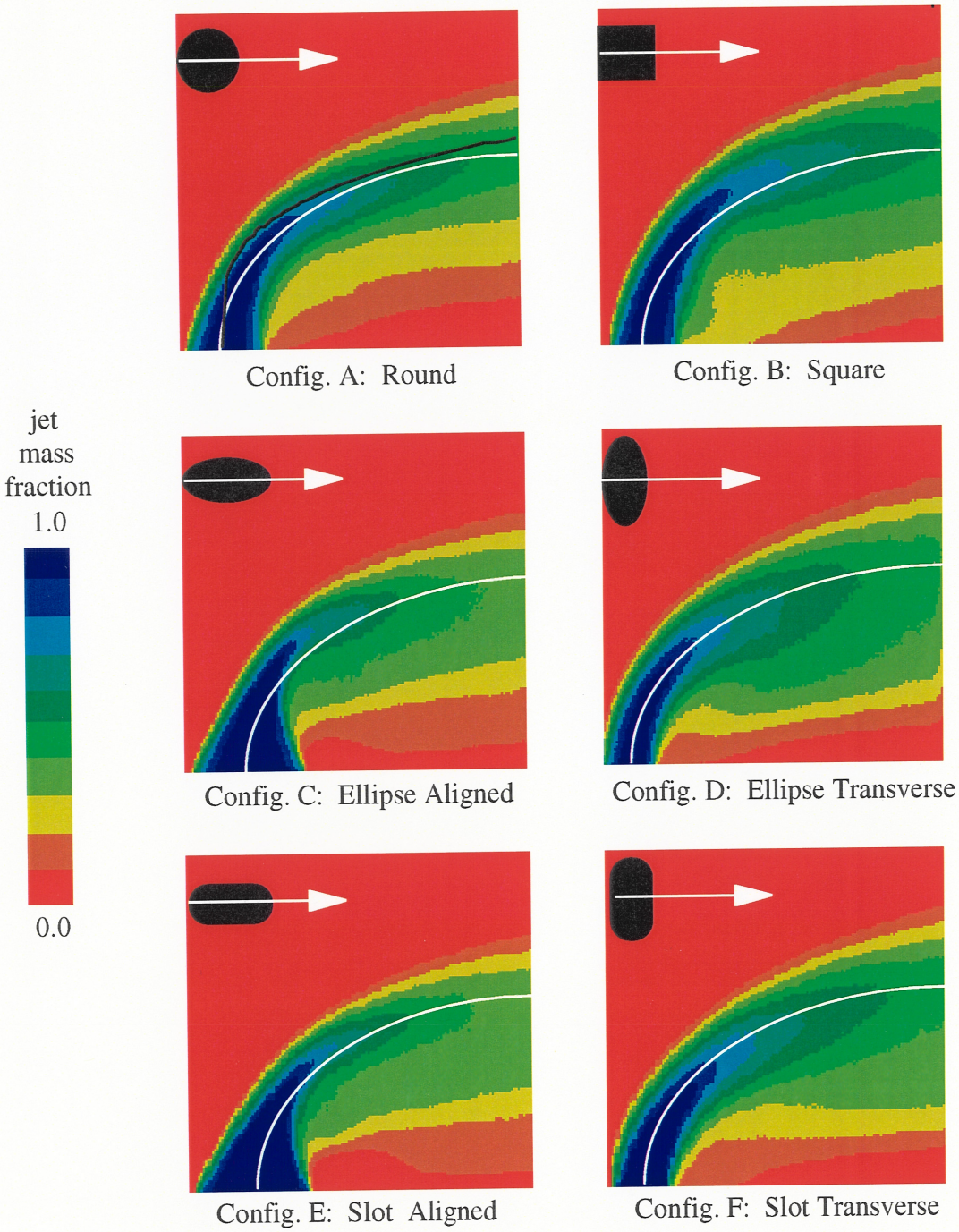

Figure 4.7-2: Side View of the Average Jet Mixture Fraction Distribution for the Six Orifice Configurations in Table 1 (left side of each figure is x/d = 0, right side is x/d = 5.5, where d is the diameter of an equivalent area circle)

The white line through each figure, which starts at the orifice centerpoint and bends with the jet, is the same in each of the six plots. It corresponds to the trajectory of the round orifice, i.e. configuration A. Trajectory is defined as the line that intersects the maximum jet concentration as a function of downstream distance. The black line plotted on the round orifice data (configuration A) is the trajectory predicted by an empirical correlation reported by Holdeman[18] for the centerplane temperature trajectory of a single heated jet in crossflow:

$$z/d = 0.76\ (\rho_j/\rho_m)^{0.15}\ J^{0.52}\ (x/d)^{0.27} \qquad (4)$$

The observed trajectory bends more quickly than the prediction, but overall the agreement is good. All of the configurations except C and E are quite similar in trajectory and overall flow features. Configurations C and E are slightly different in trajectory and in the wake region directly behind the jet. These configurations have slower mass addition due to their longer axial length. If the origin of the trajectory curve was moved nearer to the leading edge, instead of at the orifice midpoint, the same trajectory curve would closely approximate all of the configurations.

In order to study mixing performance, end-on views (planar cross sections of the flowfield perpendicular to the mainstream flow direction) were acquired at several downstream locations for each orifice configuration. In fig. 4.7-3 the jet mixture fraction distributions of the configurations shown in Table 4.7-1 are compared at 4 downstream positions using a 10 color contour plot to represent jet mixture fraction. In these plots only the jet/mainstream mixing region is shown. The downstream position is indicated on the figure as a non-dimensionalized distance where the axial distance is normalized by the orifice diameter (x/d). For the non-circular orifices the equivalent round orifice diameter is used for normalization. The primary difference between the distributions is the rate of development of the counterrotating vortices. The development is the most rapid in configurations C and E, the aligned ellipse and aligned slot, followed by the circle, square, and transvers ellipse and slot. It is surprising that although the development of vorticity appear to be quite different, the overall degree of mainstream entrainment, i.e. mixing performance, appears to be similar in each case. Apparently although low mainstream blockage increases the degree of counterrotating vorticity, the slower mass addition rate is offsetting. Therefore the net entrainment as a function of downstream distance is equivalent.

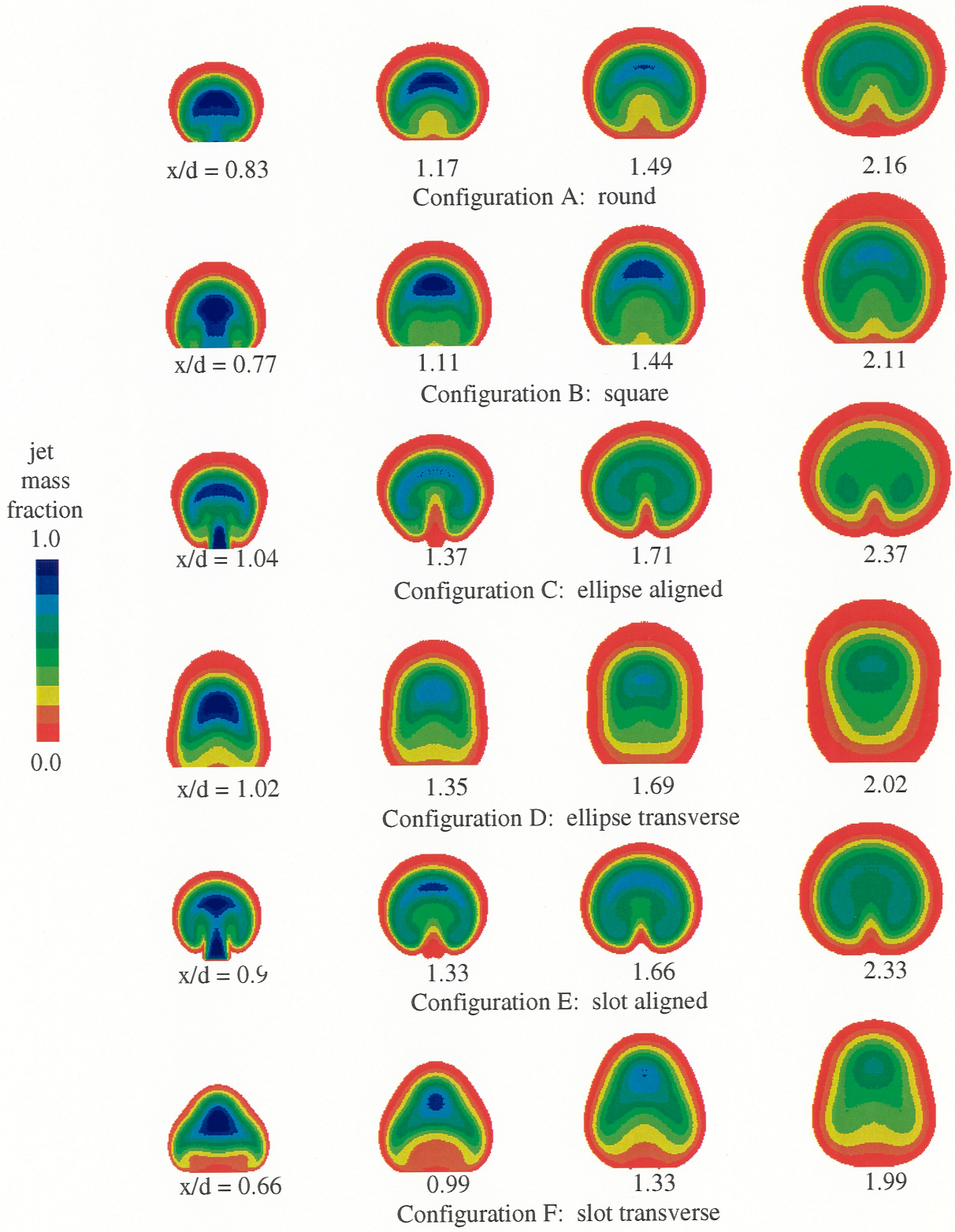

Figure 4.7-3: Comparison of End-on Jet Mixture Fraction Distributions (axial locations are non-dimensionalized by d, the equivalent round orifice diameter)

The results of the methane tracer analysis are shown in Fig. 4.7-4 for the first 4 orifice configurations. The plotting is the same as in Fig. 4.7-3. Note the spatial resolution is very coarse, but the overall qualities of the flowfield are still apparent. In general the agreement of the two data sets is very good. The ordering of development of vorticity is shown to be the same and the net mixing performance is seen to be quite similar.

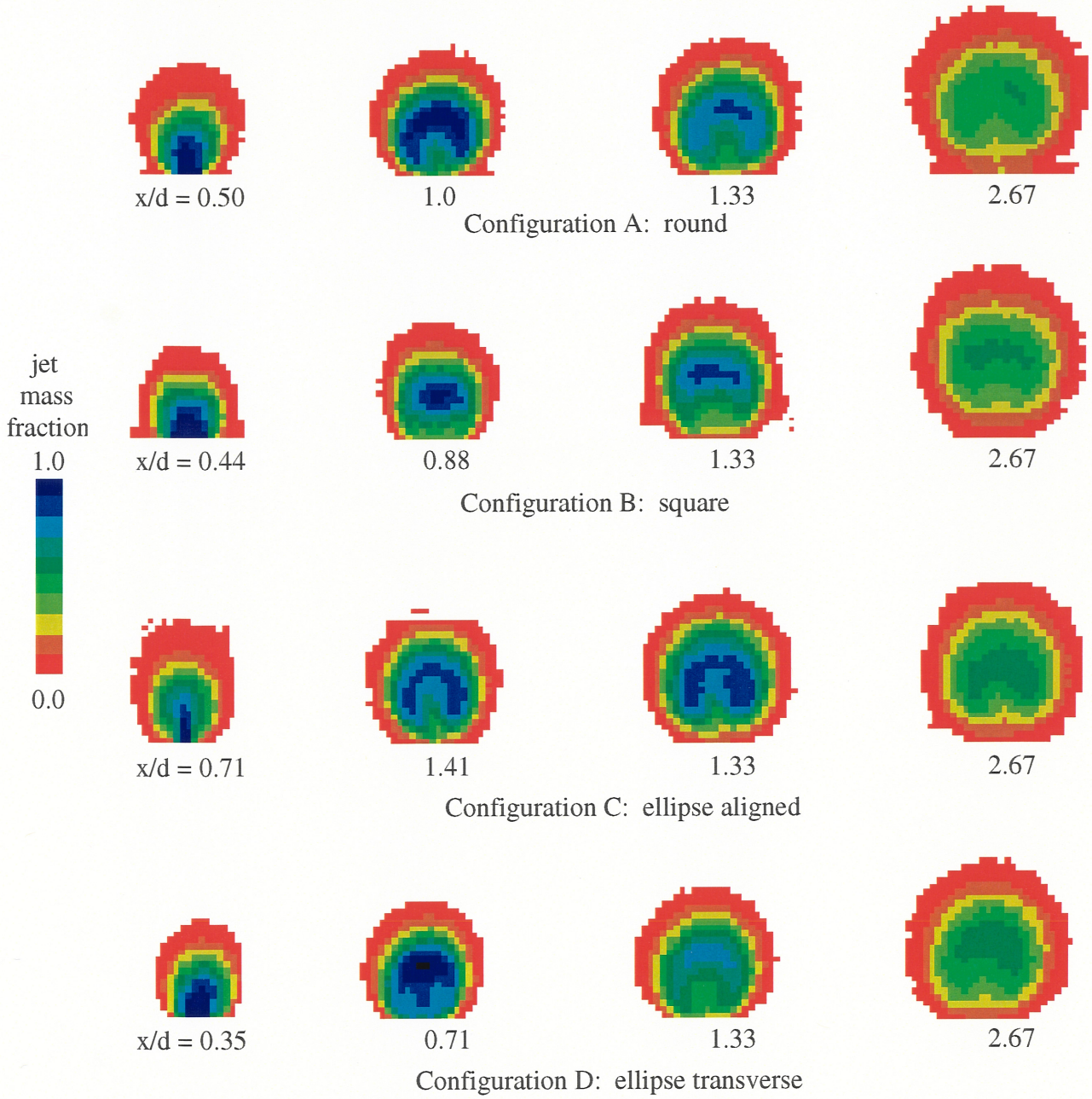

Figure 4.7-4: Comparison of Jet Mixture Fraction Distributions (gas sampling) (axial locations are non-dimensionalized by d, the equivalent round orifice diameter

Spatial unmixedness as a function of downstream position for the configurations in Table 4.7-1 are shown in Figs. 4.7-5a and 4.7-5b. These curves agree with the conclusions reached by comparison of the distributions shown in figs. 4.7-3 and 4.7-4. Although the mixing rates are slightly different, they are not substantially different.

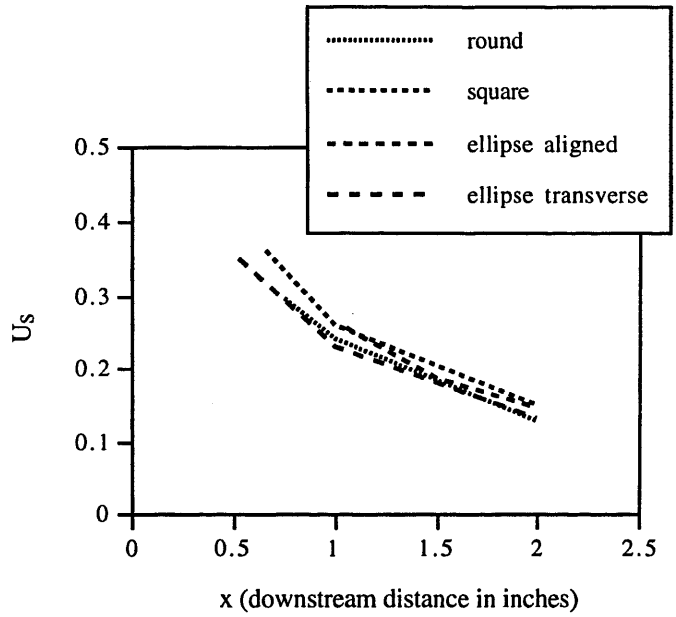

Figure 4.7-5a: Comparison of the Spatial Unmixedness of Circular and Noncircular Orifices (configurations A - D)

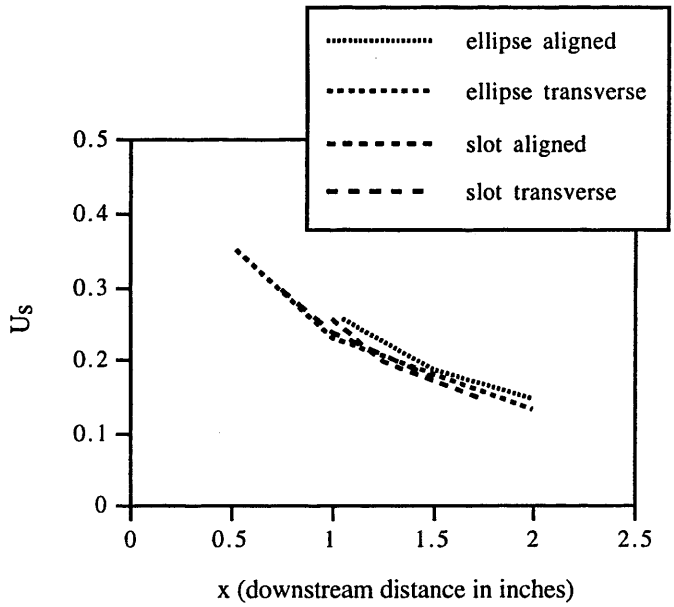

Figure 4.7-5b: Comparison of the Spatial Unmixedness of Elliptical and Slot Orifices (configurations C - F)

To further characterize the flowfield and investigate the fluctuating properties, a hot-wire anemometer was used to measure the turbulence intensity in the streamwise direction at several downstream planes for all of the configurations in Table 4.7-1. The wire was oriented in the y-z plane

and is horizontal to the flow. Turbulence intensity is defined as the rms velocity/mean velocity. In Fig. 4.7-6 the results are presented as contour plots where red represents the highest fluctuations (60%) and black the lowest. The figures represent 6.4 cm x 6.4 cm areas centered around the orifice with the bottom of the figure starting at the injection plane (z = 0).

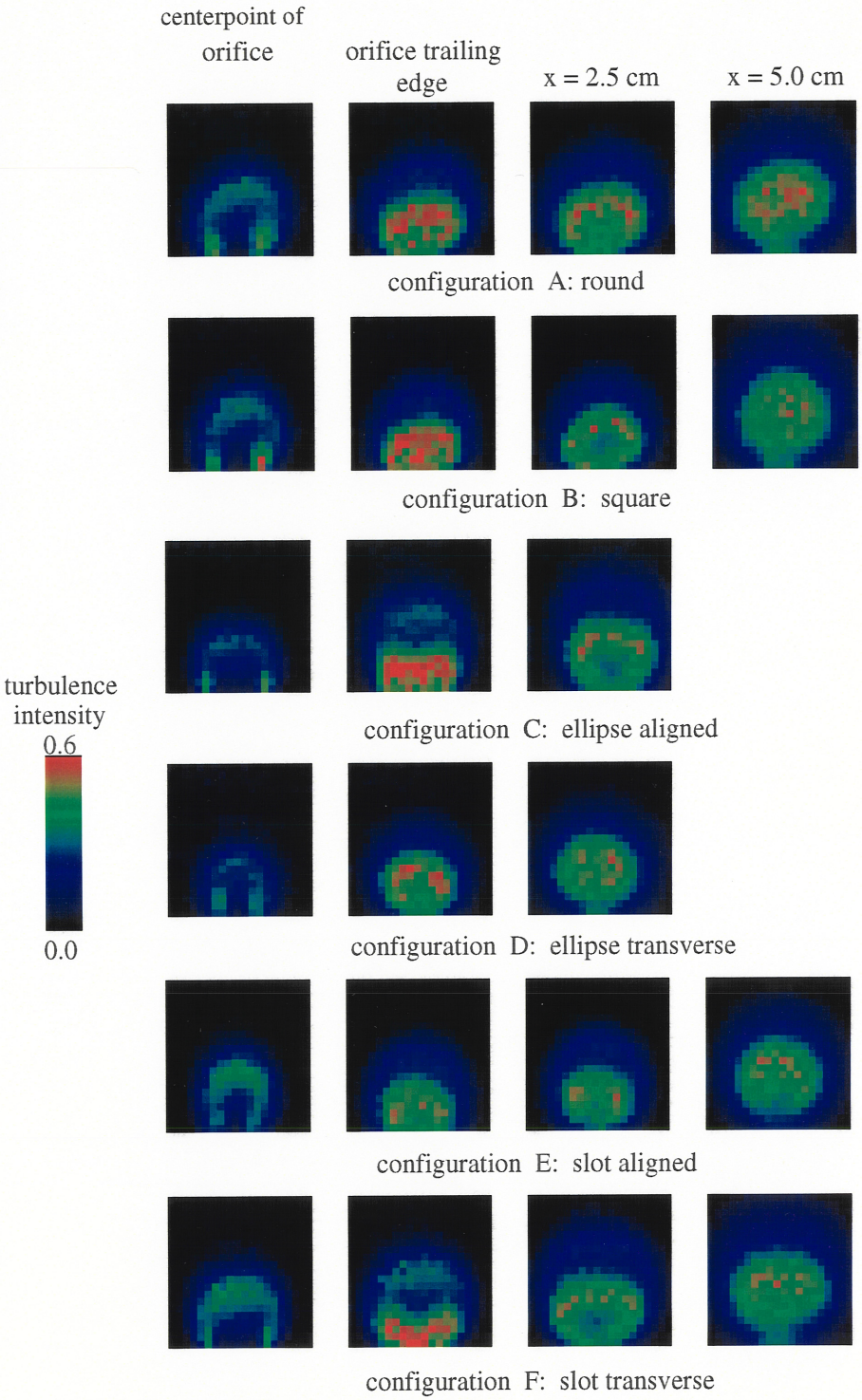

Figure 4.7-6: Turbulence Intensity Distributions for the Six Orifice Configurations in Table 4.7-1

At the first downstream station, which is a plane through the center of the orifice, the highest levels, which are about 20%, are at the interface of the jet and mainstream. Fluctuations in the core regions directly above the jet are low. The levels and distributions are independent of the configuration. At the trailing edge very high levels are indicated in the wake region for each configuration. Since velocity component were only resolved in one plane, these measurements are probably biased by intermittency and recirculation in that region. Farther downstream at the 2.5 cm and 5 cm locations the distributions becomes symmetric about the orifice centerplane and the highest flucuations are now centered in the plume of the jet. It is surprising that the overall agreement between the configurations is so similar. This would indicate that on average each of the configuration generates similar vorticity in the streamwise direction. The result is consistent with the similarity in entrainment rates indicated by the concentration distributions.

4. Conclusions

- As found in previous studies by Holdeman, mixing effectiveness can be characterized by:

$$C = (S/H) * \sqrt{J}$$

  The optimum value obtained for C for opposed inline round holes in this study was about 2.5.

- For opposed rows of round holes with centerlines inline, compared at x/H = 0.5, mixing was similar for blockages ranging from 0.59 to 0.89.

- Lower levels of U_S were obtained as a function of downstream distance when the diameter, or length, of the orifice was minimized.

- Based on the mean concentration distributions, turbulent mixing was not affected significantly by the orifice shapes that were tested.

- Mean concentration trajectories are similar independent of orifice shape.

- Inlet flow boundary conditions of both the jet and mainstream affect mixing performance.

5. References

1. Shaw, R.J., "Engine Technology Challenges for a 21st Century High Speed Civil Transport," *AIAA 10th International Symposium on Air Breathing Engines*, September 1-6, 1991 (also NASA TM 104361).

2. Jones, R.E., "Gas Turbine Engine Emissions - Problems, Progress and Future", *Prog. Energy Combust. Sci.*, vol. 4, pp. 73-113, 1978.

3. Holdeman, J.D., "Mixing of Multiple Jets with a Confined Subsonic Crossflow," *Prog. Energy Combust. Sci.*, **19**, p31-70, 1993 (also AIAA 91-2458, June 1991 and NASA TM 104412).

4. Bain, D., B. and Smith, C.E., "Analysis of Combustion Systems: Final Report," CFD Research Corportation, Huntsville, AL, Aug. 1996 (Controlled Distribution report HSR043 prepared under NASA Contract NAS 5-25967).

5. Bain, D.B., Smith, C.E., and Holdeman, J.D., "CFD Assessment of Orifice Aspect Ratio and Mass Flow Ratio on Jet Mixing in Rectangular Ducts," AIAA 94-0218, (also NASA TM 106434), Jan. 1994.

6. Bain, D.B., Smith, C.E., and Holdeman, J.D., "CFD Mixing Analysis of Axially Opposed Rows of Jets Injected into a Confined Crossflow," AIAA 93-2044, (also NASA TM 106179), June 1993.

7. Bain, D.B., Smith, C.E., and Holdeman, J.D., "CFD Mixing Analysis of Jets Injected from Straight and Slanted Slots into Confined Crossflow in Rectangular Ducts," AIAA 92-3087, (also NASA TM 105699), July 1992.

8. Blomeyer, M.M., Krautkremer, B.H., and Hennecke, D.K., "Optimum Mixing for a Two-side Injection from Opposing Rows of Staggered Jets into a Confined Crossflow", ASME paper 96-GT-453, June 1996.

9. Doerr, Thomas "Ein Beitrag zur Reduzierung des StickoxydausstoBes von Gasturbinenbrennkammern - Die Optimierung des Mischungsprozesses der Fet-Mager-Stufenverbrennung," Ph.D. Thesis, Darmstadt, 1995.

10. Doerr, Th., Blomeyer, M.M., and Hennecke, D.K., "Optimization of Multiple Jets Mixing with a Confined Crossflow," ASME paper 95-GT-313, 1995.

11. Doerr, Th., Blomeyer, M.M., and Hennecke, D.K., "Experimental Investigation of Optimum Jet Mixing Configurations for RQL-Combustors," 12th ISABE, Melbourne, Australia, 1995.

12. Doerr, Th. and Hennecke, D.K., "The Mixing Process in the Quenching Zone of the Rich-Lean Combustion Concept," AGARD-PEP 81st Symposium of Fuels and Combustion Technology for Advanced Aircraft Engines, 1993.

13. Hatch, M.S., Sowa, W.A., and Samuelsen, G.S., "Influence of Geometric and Flow Variation on Jet Mixing and NO Formation in a Model Staged Combustor with Eight Orifices," NASA contractor Report 194473, June 1996.

14. Hatch, M.S., Sowa, W.A., Samuelsen, G.S., and Holdeman, J.D., "Jet Mixing Into a Heated Cross Flow in a Cylindrical Duct: Influence of Geometry and Flow Variations," AIAA 92-0773, (also NASA TM 105390) , Jan. 1992.

15. Hatch, M.S., Sowa, W.A., Samuelsen, G.S., and Holdeman, J.D., "Influence of Geometry and Flow Variations on NO Formation in the Quick Mixer of a Staged Combustor," NASA TM 105639, July 1992.

16. Holdeman, J. D., Liscinsky, D. S., and Bain, D.B., "Mixing of Multiple Jets With a Confined Subsonic Crossflow: Part II - Opposed Rows of Orifices in Rectangular Ducts," NASA TM 107417, Feb. 1997.

17. Holdeman, J. D., Liscinsky, D. S., Oechsle, V. L., Samuelsen, G. S., and Smith, C. E. (1996). Mixing of Multiple Jets With a Confined Subsonic Crossflow in a Cylindrical Duct. Accepted for publication in *Journal of Engineering for Gas Turbines and Power* (also ASME Paper 96-GT-482 and NASA TM 107185).

18. Holdeman, J.D., "Correlation for Temperature Profiles in the Plane of Symmetry Downstream of a Jet Injected Normal to a Crossflow," NASA TN D-6966, 1972.

19. Kroll, J.T., Sowa, W.A., and Samuelsen, G.S., "Optimization of Orifice Geometry for Cross-flow Mixing in a Cylindrical Duct," NASA Contractor Report 195375, Sept. 1996.

20. Kroll, J.T., Sowa, W.A., Samuelsen, G.S., and Holdeman, J.D., "Optimization of Circular Orifice Jets Mixing into a Heated Crossflow in a Cylindrical Duct," AIAA 93-0249, (also NASA TM 105984), Jan. 11-14, 1993.

21. Kroll, J.t., Sowa, W.A., and Samuelsen, G.S., "Optimization of Orifice Geometry for Cross-Flow Mixing in a Cylindrical Duct", UCICL-ARTR-93-4, University of California, Irvine, July 1993.

22. Leong, M.L. and Samuelsen, G.S., "Quick Mixing Studies Under Reacting Flow Conditions," NASA Contractor Report 195375, September 1996.

23. Liscinsky, D.S., True, B., and Holdeman, J.D., "Mixing Characteristics of Directly Opposed Rows of Jets Injected Normal to a Crossflow in a Rectangular Duct," AIAA-94-0217, Jan. 1994.

24. Liscinsky, D.S., True, B., and Holdeman, J.D., "Experimental Investigation of Crossflow Jet Mixing in a Rectangular Duct," AIAA 93-2037, (also NASA TM 106152), June 1993.

25. Liscinsky, D.S., True, B., Vranos, A., and Holdeman, J.D., "Experimental Study of Cross-Stream Mixing in a Rectangular Duct," AIAA Paper 92-3090, (also NASA TM 106194), July 1992.

26. Oeschsle, V.L. and Conner, C.H.," Mixing and NOx Emission Calculation of Confined Reacting Jet Flows in Cylindrical and Annular Ducts," Allison Engine Company, Indianapolis, IN, April 1995 (LER report HSR021 prepared under NASA Contract NAS 3-25950, Task Order 1).

27. Oeschsle, V.L.," Mixing and NOx Emission Calculation of Confined Reacting Jet Flows in a Cylindrical Duct," Allison Engine Company, Indianapolis, IN, August 1995 (LER report HSR005 prepared under NASA Contract NAS 3-25950, Task Order 1).

28. Rosfjord, T.J. and Padget, F.C., "Experimental Assessment of the Emissions Control Potential of a Rich/Quench/Lean Combustor for High Speed Civil Transport Aircraft Engines," United Technologies Research Center, E. Hartford, CT, April 1996 (Pratt & Whitney LER Report HSR032 prepared under Contract NAS 3-25952, Task Order 3).

29. St. John, D. and Samuelsen, G.S., "Detailed Studies of the Quick Mixing Region in Tich Burn Low NOx Combustors," University of California, Irvine Combustion Laboratory, Irvine CA (LER Report HSR048 prepared under Pratt & Whitney P.O. No. 0865124 and NASA Grant NAG 3-1110).

30. Smith, C.E., Talpallikar, M.V., and Holdeman, J.D., "A CFD Study of Jet Mixing in Reduced Areas for Lower Combustor Emissions," AIAA Paper 91-2460, (also NASA TM 104411), June 1991.

31. Sowa, W.A., Kroll, J.T., Samuelsen, G.S., and Holdeman, J.D, "Optimization of Orifice Geometry for Cross-Flow Mixing in a Cylindrical Duct," AIAA 94-0219, (also NASA TM 106436), Jan. 1994.

32. Talpallikar, M.V., Smith, C.E., Lai, M.C., and Holdeman, J.D., "CFD Analysis of Jet Mixing in Low NOx Flametube Combustors," *J. Eng. Gas Turbine Pwr.*, **114**, 416, 1992, (also ASME 91-217 and NASA TM 104466, 1991).

33. Vranos, A., Liscinsky, D.S., True, B., and Holdeman, J.D., "Experimental Study of Cross-Stream Mixing in a Cylindrical Duct," AIAA 91-2459, (also NASA TM 105180), June 1991.

34. Danckwertz, P.V., "The Definition and Measurement of Some Characteristics of Mixtures," Appl. Sci. Res., Sec. A, Vol. 3, pp. 279-296, 1952.

35. Ho, C.-M, and Gutmark, E., "Vortex Induction and Mass Entrainment in a Small-Aspect-Ratio Elliptic Jet," *J. Fluid Mech.*, **179**, pp383-405, 1987.

36. Gutmark, E. and Ho, C.-M., "Visualization of a Forced Elliptic Jet, *AIAA J.*, **24**, pp. 684-685, 1986.

37. Gutmark, E. and Schadow, K.C., "Flow Characteristics of Orifice and Tapered Jets," *Phys. Fluids*, **30** (11), pp. 3448-3454, November 1987.

38. Quinn, W.R., "On Mixing in an Elliptic Turbulent Free Jet," *Phys. Fluids*, **A 1** (10), pp. 1716-1722, October 1989.

39. Wu, J.M., Vakili, A.D., and Yu, F.M., "Investigation of the Interacting Flow of Nonsymmetric Jets in Crossflow," *AIAA Journal*, **26** (8), pp. 940-947, August 1988.

REPORT DOCUMENTATION PAGE

Form Approved
OMB No. 0704-0188

Public reporting burden for this collection of information is estimated to average 1 hour per response, including the time for reviewing instructions, searching existing data sources, gathering and maintaining the data needed, and completing and reviewing the collection of information. Send comments regarding this burden estimate or any other aspect of this collection of information, including suggestions for reducing this burden, to Washington Headquarters Services, Directorate for Information Operations and Reports, 1215 Jefferson Davis Highway, Suite 1204, Arlington, VA 22202-4302, and to the Office of Management and Budget, Paperwork Reduction Project (0704-0188), Washington, DC 20503.

1. AGENCY USE ONLY (*Leave blank*)

2. REPORT DATE
June 2003

3. REPORT TYPE AND DATES COVERED
Final Contractor Report

4. TITLE AND SUBTITLE
Enhanced Mixing in a Rectangular Duct

5. FUNDING NUMBERS
WBS–22–714–01–38
NAS3–25954, Task Order 12

6. AUTHOR(S)
D.S. Liscinsky and B.True

7. PERFORMING ORGANIZATION NAME(S) AND ADDRESS(ES)
Pratt & Whitney
United Technologies Research Center
400 Main Street
East Hartford, Connecticut 06108

8. PERFORMING ORGANIZATION REPORT NUMBER
E–13907

9. SPONSORING/MONITORING AGENCY NAME(S) AND ADDRESS(ES)
National Aeronautics and Space Administration
Washington, DC 20546–0001

10. SPONSORING/MONITORING AGENCY REPORT NUMBER
NASA CR—2003-212320

11. SUPPLEMENTARY NOTES
This reseach was originally published internally as HSR047 in March 1997. Project Manager, James D. Holdeman, Turbomachinery and Propulsion Systems Division, NASA Glenn Research Center, organization code 5830, 216–433–5846.

12a. DISTRIBUTION/AVAILABILITY STATEMENT
Unclassified - Unlimited
Subject Category: 07 Distribution: Nonstandard
Available electronically at http://gltrs.grc.nasa.gov
This publication is available from the NASA Center for AeroSpace Information, 301–621–0390.

12b. DISTRIBUTION CODE

13. ABSTRACT ***(Maximum 200 words)***
An experimental investigation of the mixing of non-reacting opposed rows of jets injected normal to a confined rectangular crossflow has been conducted. Planar Mie-scattering was used to measure the time-average concentration distribution of the jet fluid in planes perpendicular to the duct axis. Particular emphasis was placed on the study of closely spaced orifice configurations applicable to the mixing zone of an RQL combustor. Baseline studies were performed of mixing under "ideal" conditions, i.e., plenum fed jets injecting into a crossflow uniform in velocity and turbulence intensity. In addition, more practical ("non-ideal") issues encountered during hardware design were also studied. As in other studies, mixing effectiveness, determined using a spatial unmixedness parameter based on the variance of mean jet concentration distributions, was found to be optimum when the spacing-to-duct-height ratio was inversely proportional to the square root of the jet-to-mainstream momentum-flux ratio. This relationship is suitable for design under ideal flow conditions. Inlet flow boundary conditions of the jet and approach flow (mainstream) were found to strongly influence mixing performance, but no attempt was made to determine optimum performance under non-ideal conditions. The tests performed do offer some guidance as to expected mixing behavior for several common variables likely to be imposed by hardware constraints. Additionally, in this study it was found that for rows of orifices with opposite centerlines inline, mixing was similar for blockages up to 89 percent (previous crossflow mixing studies concerned with dilution zone configurations, blockages were typically less than 50 percent). Lower levels of unmixedness were obtained as a function of downstream location when axial injection length was minimized. Mixing may be enhanced if orifice centerlines of opposed rows are staggered, but blockage must be ≤50 percent in this configuration. Round hole and "square" orifice shapes had similar performance. Other variations in orifice shape did not substantially augment overall mixing performance. Furthermore an isothermal mixing data set was generated and used by CFDRC as input to a NO_x inference code.

14. SUBJECT TERMS
Gas turbine; Combustor; RQL; Mixer; Jet-in-crossflow; Non-reacting

15. NUMBER OF PAGES
50

16. PRICE CODE

17. SECURITY CLASSIFICATION OF REPORT	18. SECURITY CLASSIFICATION OF THIS PAGE	19. SECURITY CLASSIFICATION OF ABSTRACT	20. LIMITATION OF ABSTRACT
Unclassified	Unclassified	Unclassified	